Atmos. Chem. Phys. Discuss., 7, 2197–2248, 2007
www.atmos-chem-phys-discuss.net/7/2197/2007/
© Author(s) 2007. This work is licensed
under a Creative Commons License.

Atmospheric Chemistry and Physics Discussions

# Model study of the cross-tropopause transport of biomass burning pollution

**B. N. Duncan**[1,2], **S. E. Strahan**[1,2], **and Y. Yoshida**[1,2]

[1]Goddard Earth Sciences and Technology Center, University of Maryland, Baltimore County, Baltimore, Maryland, USA
[2]The Atmospheric Chemistry and Dynamics Branch, NASA Goddard Space Flight Center, Greenbelt, Maryland, USA

Received: 25 January 2007 – Accepted: 12 February 2007 – Published: 15 February 2007

Correspondence to: B. N. Duncan (bryan.n.duncan.1@gsfc.nasa.gov)

## Abstract

We present a modeling study of the troposphere-to-stratosphere transport (TST) of pollution from major biomass burning regions to the tropical tropopause layer (TTL) and lower stratosphere (LS). We show that biomass burning pollution regularly and significantly impacts the composition of the TTL/LS. TST occurs through 1) slow ascent in the TTL and 2) quasi-horizontal exchange in the regions of the subtropical jets; we find both pathways to be important. The seasonal oscillation in CO in the TTL/LS (i.e., the CO "tape recorder") is caused largely by seasonal changes in biomass burning. Another contributing factor is the long-range transport of northern hemispheric pollution (e.g., biofuels and fossil fuels) to the northern tropics in boreal winter. Other tropical sources of CO (e.g., methane oxidation) have insignificant seasonal variation, contributing little to the tape recorder. Interannual variation of CO in the TTL/LS is caused by year-to-year variations in biomass burning and the strength, frequency, and locations of deep convection, which lofts pollution to the upper troposphere. During our study period, 1994–1998, we find that the highest concentrations of CO in the TTL/LS occur during the strong 1997/98 El Niño event for two reasons: i. tropical deep convection was stronger and ii. emissions were higher. This extreme event can be seen as an upper bound on the impact of biomass burning pollution on the TTL/LS. We estimate that the 1997 Indonesian wildfires increased CO in the entire TTL and tropical LS (<60 mb) by more than 40% and 10%, respectively, for several months. Zonal mean ozone increased and the hydroxyl radical decreased by as much as 20%, increasing the lifetimes and, subsequently TST, of trace gases. Our results indicate that the impact of biomass burning pollution on the TTL/LS is likely greatest during an El Niño event due to favorable dynamics and historically higher burning rates.



ACPD

7, 2197–2248, 2007

## 1 Introduction

Schoeberl et al. (2006) identified the stratospheric "tape recorder" in carbon monoxide (CO), a seasonal oscillation in tropical lower stratospheric CO, in the Aura Microwave Limb Sounder (MLS) data. The term "tape recorder" was coined to describe the seasonal progression of tropical water vapor observed by the Upper Atmosphere Research Satellite (UARS) (Mote et al., 1996, Randel et al., 2001). Unlike the water vapor tape recorder which is controlled by seasonal variation in tropical upper tropospheric temperatures, Schoeberl et al. found that the CO tape recorder is linked to seasonal biomass burning, closely following the two maxima in the tropics that occur around March and September of each year (Duncan et al., 2003a). The main objectives of this modeling study are to discuss the troposphere-to-stratosphere transport (TST) of trace gases from biomass burning and to assess the impact of the pollutants on the chemistry of the upper troposphere (UT) and lower stratosphere (LS). For this work, we use the Global Modeling Initiative's (GMI) combined stratosphere-troposphere chemistry and transport model (COMBO CTM).

Biomass burning pollution is often lofted by convection to the UT (e.g., Pickering et al., 1996), where it can enter the tropical tropopause layer (TTL), a region above the typical maximum vertical extent of convection (∼150 mb) and below the tropopause (∼100 mb). Vertical motions to the tropopause in the TTL are associated with slow, large-scale ascent due to clear sky radiative heating (Folkins et al., 1999), which varies seasonally with, for instance, temperature and ozone (e.g., Folkins et al., 2006). The level of zero radiative heating (LZH) in the TTL at ∼125 mb is generally lower near the equator and areas of frequent deep convection (Gettelman et al., 2004; Folkins et al., 2006). The LZH is most sensitive to water vapor, though it is also sensitive to ozone and carbon dioxide (Gettelman et al., 2004). Aerosols also impact the radiative budget of the troposphere directly and indirectly by modifying clouds. Consequently, biomass burning pollutants have the potential to impact the dynamics of the TTL/LS, including TST.



ACPD
7, 2197–2248, 2007

Newell and Gould-Stewart (1981) postulated the existence of a "stratospheric fountain", an area where tropospheric air preferentially enters the stratosphere, over Indonesia and India during their respective monsoon seasons. Their hypothesis has generated considerable debate over the existence of a fountain (e.g., Dessler, 1998; Sherwood, 2000; Hatsushika and Yamazaki, 2003). Fueglistaler et al. (2004), using trajectory calculations, found that 80% of their trajectories that ascended to the LS entered the TTL over the western Pacific "Warm Pool", an area with high sea surface temperatures (SSTs) and deep convection. The air in the TTL typically resides there for several weeks and travels ~5000–10 000 km before crossing the tropopause. The preferred locations of TST are the western Pacific Ocean, India, and the Indian Ocean.

Biomass burning pollution has been observed to be transported by the southern subtropical jet (e.g., Folkins et al., 1997; Chatfield et al., 2002; Staudt et al., 2002), where it can enter the lowermost stratosphere (LMS; i.e., the region below the 380 K potential temperature surface, but above the extra-tropical tropopause), via quasi-horizontal exchange (Holton et al., 1995). The subtropical jets meander around the globe varying in altitude, latitude, and intensity; therefore, the locations, frequencies, etc. of TST via this pathway will vary.

During winter, a strong gradient in potential vorticity creates a barrier to mixing across the subtropical jet. In summer, PV gradients are much weaker and transient wave disturbances can grow in amplitude, break, and cause irreversible mixing between the tropical UT and the LMS. Such disturbances are common in the northern summer near the Asian and Mexican monsoon circulations and allow significant exchange between the tropics and midlatitudes between 100–200 mb (Chen, 1995). However, the LMS is characterized by descending air, so that most of the pollution will eventually return to the troposphere (Schoeberl et al., 2004).

Li et al. (2005) and Fu et al. (2006) showed that MLS CO is high over the Tibetan Plateau during the Indian monsoon in summer. The lofting of pollution to the UT during the Asian monsoon is also evident in the MOPITT CO data (Kar et al., 2004). Fu et al. (2006) discussed a different mechanism than Dethof et al. (1999) for the transport

of water vapor and polluted air to the stratosphere via convective transport over the plateau. They found that convection over the plateau is deeper than over the monsoon area, detraining more air near the tropopause. That is, this pathway is a short-circuit to the normal pathway of slow ascent in the TTL.

We do not believe that direct injection of biomass burning pollution above the tropical tropopause via convection is an important transport pathway. Liu and Zipser (2005) analyzed five years of TRMM data, concluding that 1.3% of tropical convection systems reach 14 km and 0.1% possibly penetrates the tropopause (i.e., 380 K potential temperature). They found that overshooting deep convection occurs predominantly over central Africa, but also over Indonesia and South America. Fueglistaler et al. (2004) found that deep convection penetrating the tropopause is a very small contributor to TST. To our knowledge, pyro-cumulonimbus injection into the tropical LS has not been observed as it has in the boreal regions where the tropopause is lower (e.g., Livesey et al., 2004, Fromm et al., 2005).

Despite local zones of deep convection penetrating the stratosphere, tropical convective systems are not responsible for depositing pollutants at the tropopause. Instead, convective systems largely die out at 350 K and large-scale ascent in the TTL brings air up to the tropical LS (i.e., ≥380 K). The success of the COMBO CTM in reproducing the CO tape recorder as discussed in Schoeberl et al. (2006) demonstrates that this tool is appropriate to investigate the tropical TST process. MLS CO observations in the UT/LS region may provide us with additional insight.

In this paper, we will show that biomass burning pollution does indeed reach the LS, changing the composition of chemically and radiatively important trace gases there. In Sect. 2, we describe the COMBO CTM and the meteorological fields used to drive its transport. We present a model evaluation in Sect. 3. In Sect. 4, we identify the major TST pathways of biomass burning pollution using the 1997 Indonesian fires as an example; we assess the impact of the pollution on the composition of the UT/LS. In Sect. 5, we estimate the contributions of pollution from several source regions, including interannual variability (IAV), to the CO tape recorder. A summary of conclusions is

given in Sect. 6.

## 2 Global modeling initiative Combined Stratosphere-Troposphere CTM

The COMBO CTM was developed from the stratospheric CTM described by Rotman et al. (2001). Initial descriptions of the COMBO CTM can be found in Ziemke et al. (2006). Strahan et al. (2007) and references therein describe the stratospheric processes in the model.

### 2.1 Chemistry

The chemical mechanism is obtained by combining tropospheric and stratospheric mechanisms and includes 117 species, 322 chemical reactions, and 81 photolysis reactions. The chemical mass balance equations are integrated using the SMVGEAR II algorithm (Jacobson, 1995). The tropospheric mechanism includes a detailed description of tropospheric $O_3$-$NO_x$-hydrocarbon chemistry (Bey et al., 2001). It has been updated with recent experimental data from Tyndall et al. (2001), Sander et al. (2003), and Atkinson et al. (2003), and data for the quenching reactions of $O(^1D)$ by $N_2$, $O_2$, and $H_2O$ (Ravishankara et al., 2002; Dunlea and Ravishankara, 2004). The stratospheric mechanism is described in Kinnison et al. (2001) and Douglass et al. (2004). A description of the polar stratospheric cloud parameterization is provided by Considine et al. (2000). Mixing ratio boundary conditions were imposed for halogen source gases for conditions appropriate for the simulation year as described in Strahan et al. (2007) and Douglass et al. (2004).

Photolysis frequencies are computed using the Fast-JX radiative transfer algorithm, which combines the Fast-J tropospheric scheme described in Wild et al. (2000) with the Fast-J2 stratospheric scheme of Bian and Prather (2002) (Michael Prather, personal communication, 2005). The algorithm treats both Rayleigh scattering as well as Mie scattering by clouds and aerosol.



ACPD
7, 2197–2248, 2007

The model simulates the radiative and heterogeneous chemical effects of sulfate, dust, sea-salt, organic carbon and black carbon aerosol on tropospheric photochemistry. The monthly-averaged aerosol surface area distributions were obtained from the Goddard Chemistry Aerosol Radiation and Transport (GOCART) model for 2001 (Chin et al., 2002). The aerosol fields were coupled to the COMBO CTM as described by Martin et al. (2003). The reaction probability for $N_2O_5$ is a function of aerosol type, relative humidity, and temperature, and is significantly lower than earlier estimates (Evans and Jacob, 2005).

### 2.2 Emissions

Table 1 summarizes the annual anthropogenic and natural emissions.

#### 2.2.1 Anthropogenic emissions

The base fossil fuel emissions are described by Bey et al. (2001) and Duncan et al. ("The global budget of CO, 1988–1997: source estimates and validation with a global model", submitted manuscript; hereafter referred to as Duncan et al., 2007) that includes $NO_x$ emissions from the Global Emission Inventory Activity (GEIA) (Benkovitz et al., 1996) and non-methane hydrocarbon (NMHC) emissions from Piccot et al. (1992). The base emissions, which are for 1985, are scaled to reflect emissions in 1995 as described in Bey et al. (2001). Seasonal variation (±10%) is applied for CO poleward of 35° N to reflect higher automobile emissions in winter (Duncan et al., 2007). The monthly mean emissions of $NO_x$ from aircraft are from the inventory of Baughcum et al. (1996) and Metwally (1995), representing 1995 conditions. Biofuel emissions are estimated from the inventory and emission factors of Yevich and Logan (2003).

For the Indonesian wildfire experiment in Sect. 4, we use the Global Fire Emissions Database version 2 (GFEDv2; Van der Werf et al., 2006). We did not simulate the radiative and heterogeneous chemical impacts of the aerosols from the Indonesian

fires. Duncan et al. (2003b) showed that they decreased OH by about 10% over much of the Indian Ocean with a concomitant increase in CO by <10%. Neglecting the effect of these aerosols on CO is not important for our study as our purpose is to estimate if the change in the composition of trace gases in the TTL and LS is substantial.

For the experiments in Sect. 5, we use the biomass burning emissions inventory presented in Duncan et al. (2003a), which represents a mean for 1980 to 1990. Categories in the inventory are deforestation, shifting cultivation, agricultural residues burned in the field, savanna burning, and forest fires. Trace gas emission factors are from Andreae and Merlet (2001).

In the inventories described here, we do not directly account for the emissions of several NMHC, such as aromatics, from fossil fuels, biofuels, and biomass burning. We estimate the production of CO from these NMHC by multiplying the emission rate of each NMHC in a given inventory by a yield of CO per carbon oxidized, as described in Duncan et al. (2007). Applying these yields, we find that oxidation of anthropogenic NMHC results in a source of CO that is 2%, 8.6% and 5% of the direct CO emission from fossil fuels, biofuels and biomass burning, respectively. The direct emissions from these three sources are increased to account for the indirect source from oxidation of co-emitted NMHC.

### 2.3 Natural emissions

The distribution of isoprene emissions from vegetation is based on a modified version of the inventory of Guenther et al. (1995) and is dependent on solar radiation and temperature. The principal modifications are described by Wang et al. (1998) and Bey et al. (2001). The global emission rate of the modified inventory is 380 Tg C/y, which is about 25% lower than the inventory of Guenther et al. (1995), 503 Tg C/y. We do not simulate the transport and chemistry of monoterpenes and methanol directly, but we do account for the CO produced from their oxidation following Duncan et al. (2007).

The lightning source is set to 5.0 Tg N/y and is horizontally distributed using monthly mean lightning emissions based on the locations and heights of deep convective clouds

from the ISCCP cloud climatology (Price et al., 1997). Lightning flash rates used in constructing these emissions are based on the cloud-top height parameterization of Price and Rind (1992). The vertical distribution of the $NO_x$ is specified by the profiles derived from cloud-resolved convection simulations of Pickering et al. (1998).

We compute emissions of NO by soil microbes as described in Wang et al. (1998). The emissions are a function of vegetation type (Olson, 1992), temperature, fertilizer usage, and precipitation history. The scheme simulates the oxidation of NO to $NO_2$ and subsequent uptake by vegetation within the canopy (Jacob and Bakwin, 1991).

#### 2.3.1 Other

Methane mixing ratios are forced at the surface with annual mean values for 2001 using National Oceanic and Atmospheric Administration (NOAA) Global Monitoring Division (GMD) measurements (Dlugokencky et al., 1998). They are zonally uniform in four semi-hemispheres. Monthly-averaged acetone concentrations are specified following Jacob et al. (2002).

### 2.4 Transport

In our study we use five years of meteorological fields from the Goddard Modeling and Assimilation Office (GMAO) GEOS-4 general circulation model (GEOS-4-GCM) (Bloom et al., 2005), using SSTs representing 1994 to 1998. They have been regridded to 42 vertical levels with a lid at 0.01 hPa; there are ~20 levels from the surface to the LS (60 mb) with ~6 levels in the TTL/LS. The horizontal resolution is 2° latitude × 2.5° longitude.

The COMBO CTM transports 71 of the 117 species in the chemical mechanism, using the advection scheme of Lin and Rood (1996). Convective transport is taken from the MATCH model (Rasch et al., 1997), which uses the following meteorological fields as input: cloud mass fluxes, entrainment and detrainment fluxes, and large-scale downwelling. Both shallow and deep convection are considered, following the

algorithms of Hack (1994) and Zhang and McFarlane (1995). The model uses the Harvard wet scavenging algorithm (Liu et al., 2001) and the dry deposition scheme described by Wang et al. (1998), which follows the methodology of Wesely et al. (1985).

## 3 Model evaluation

### 3.1 Summary of previous work

Schoeberl et al. (2006) found that the MLS CO tape recorder is similar to that of the model's, implying that tropical ascent and horizontal mixing in the model's UT/LS are credible. Ziemke et al. (2006) compared OMI/MLS tropospheric column ozone (TCO) observations with those of the model, finding that the two agree well both spatially and seasonally, including for the South Atlantic maximum and western Pacific minimum. The model is typically higher from 30–40° latitude of both hemispheres, particularly the northern hemisphere (NH), and too low over the Warm Pool in all seasons. (Ozonesonde data support that the model's TCO from 30–40° N is too high.) Strahan et al. (2007) evaluated the model's performance in the UT/LS using a variety of satellite and aircraft-derived transport diagnostics. They showed that the model has credible seasonally-varying composition and transport in the LS, including the LMS, as well as realistic coupling between the extra-tropical troposphere and stratosphere.

### 3.2 Troposphere

In this study, we use CO as a tracer of transport as its chemical lifetime is about a month in the tropics, which is typically longer than the timescales of most transport processes, including TST. The evaluation of our 5-yr model run (1994–1998 SSTs) is for CO and OH, as reaction with OH is the primary sink for CO. Our evaluation is necessarily qualitative as we use climatological emissions and the meteorology represents no particular time, though it should capture IAV associated with the phases of the El Niño/Southern Oscillation (ENSO).



ACPD
7, 2197–2248, 2007

Figure 1 shows a comparison of model CO and NOAA GMD observations for 1994–1998 (Novelli et al., 1992; 1998). Statistical information for each station is given in Table 2. The model is systematically biased low at most stations in local winter/spring when the burden is typically at an annual maximum. Transport deficiencies may play a role as the seasonal maximum in the tropics is largely due to the long-range transport of pollution from biomass burning and fossil fuel source regions. The model CO generally compares well to observations in local summer/fall when regional photochemical production of CO becomes more important. Another possible reason for the model's low bias is too high OH, though this does not appear to be the case.

The mean tropospheric OH for our simulation (1994 SSTs) is $0.98\times10^6$ molec/cm$^3$, which is similar to that reported by Spivakovsky et al. (2000), $1.16\times10^6$ molec/cm$^3$. The $CH_3CCl_3$ lifetime with respect to tropospheric OH is 6.1 y, which is similar to that reported by Prinn et al. (2005), 6.0 (+0. 5, –0.4) y, and Spivakovsky et al. (2000), 5.7 y. Though the lifetime is reasonable in our model, it is weighted toward the lower tropical troposphere, providing less information on the quality of model OH elsewhere. A known deficiency in the GEOS-4-GCM is that the tropical cloud optical depths (COD) are too thin in the middle/upper troposphere, though the column COD are similar to those from MODIS and ISCCP; this problem results because the atmosphere of the GCM is too dry (Bloom et al., 2005). The radiative effect of clouds on global mean OH is not very sensitive to the column COD, but it is to the cloud vertical distribution (H. Liu, personal communication, 2006).

There are two long-term aircraft missions, Japan Airlines (JAL; Matsueda et al., 1998) and Measurements of OZone by Airbus In-service airCraft (MOZAIC; Nedelec et al., 2005), that measure CO in the UT. Figure 2 shows a seasonal comparison of the model and the JAL data (9–13 km) from 1994–1998 for flights from Tokyo, Japan to Sydney, Australia. The data include 19 to 27 flights per season; however, we did not use data from September 1997 to May 1998 as CO was abnormally high from the Indonesian fires (Matsueda et al., 1999). The model captures the observed latitudinal gradient in mean CO and simulates much of the observed IAV. For instance, the model

and observations show IAV in the northern subtropics from March through May, a time when the UT is impacted by biomass burning pollution from Southeast Asia (e.g., Jacob et al., 2003). In the data, there is strong IAV from September through November in the southern tropics, which is associated with the IAV of biomass burning emissions; the model does not show strong IAV as we use climatological emissions. Figure 3 shows a histogram comparison of the model and MOZAIC flights between Europe and East Asia. Consistent with the GMD measurements, the data show that the model CO is often biased low, though the spatial and temporal distributions are similar to the data.

## 4 Cross-tropopause transport pathways: 1997 Indonesian wildfires

In this section, we present a COMBO CTM simulation of the 1997 Indonesian wildfires, one of the largest burning events of the 20th century, to illustrate the principal cross-tropopause pathways of biomass burning pollution. The fires began in August, peaked in September and October, and ended in November. Observations indicate that the wildfires had a profound impact on the composition of the tropical troposphere (Duncan et al., 2003b and references therein), including the UT (Matsueda et al., 1999; Matsueda and Inoue, 1999). The purposes of this experiment are 1) to identify the major TST pathways of the pollution and 2) to understand the impact of this extreme biomass burning event on the composition of the TTL/LS.

Duncan et al. (2003b) detailed the tropospheric transport pathways of the pollution. The Walker Circulation was weak and not well organized, which is typical of El Niño conditions. Consequently, the prevailing flow throughout the tropical troposphere from Africa to the Indian Ocean was characterized by weak, recirculating easterlies, which allowed most of the pollution to remain over the tropical Indian Ocean through November. Transport to the UT via deep convection mixed the pollution throughout the troposphere over the tropical Indian Ocean. We find similar transport pathways in the simulation presented here.

Duncan et al. (2003b) could not determine if the pollution transported to the LS

was realistic; transport in their model was driven by assimilated meteorology, which was known to cause excessive stratosphere-troposphere exchange (STE), a common problem of assimilated fields (e.g., Douglass et al., 2003; Schoeberl et al., 2003). Here, we use GEOS-4-GCM meteorological fields (1997 SSTs), which have reasonable STE, to drive transport in the COMBO CTM. As the ENSO phenomenon is largely driven by SSTs, our simulation captures the major meteorological features associated with this historic El Niño. For instance, the locations of tropical precipitation agree reasonably well with the distributions from the Global Precipitation Climatology Project (GPCP) for August through November 1997 (Adler et al., 2003). The model and observed precipitation are higher than climatology (1979–1999) over the central/eastern Pacific and western Indian Oceans, and lower over the Maritime continent and eastern Indian Ocean, which are characteristics of the El Niño phase (Dai and Wigley, 2000).

In Sects. 4.1–4.2, we present the results of two model simulations, with and without the Indonesian wildfire emissions. We refer to the difference in trace gas concentrations between the two runs as perturbations caused by the wildfires.

### 4.1 Transport pathways within the TTL and LS

The cross-tropopause transport of the wildfire's pollution occurs by slow ascent in the TTL, especially over the Indian Ocean, and quasi-horizontal exchange in the subtropical jet regions, especially the southern jet. The two TST pathways are both important in our model.

#### 4.1.1 Quasi-horizontal exchange

In general, the maximum extent of the convective upward mass flux in our model is ~200 mb. While advective flow in the tropical UT is characterized by weak, recirculating easterlies, westerly flow in the subtropical jets (>20° N and >20° S) is relatively strong, especially the southern jet as it is seasonally stronger (Fig. 4). Flow throughout the TTL is similar to that shown in Fig. 4.

Figure 5 shows the monthly-averaged CO perturbation (%) at 200 mb for August through November. The bulk of the CO remains over the tropical Indian Ocean in all four months, where the perturbation is >100% over much of the region. In August and September, the pollution is transported by the tropical easterly jet, which weakens in October and November as the Asian monsoon circulation breaks down. The figure shows that pollution is peeled away by the subtropical jets, especially the southern jet, from the main plume over the Indian Ocean in September and October, rapidly circling the globe (Figs. 5c–d).

The importance of the subtropical jets as TST pathways to the LMS is seen in Fig. 6, which shows the CO perturbation (%) in October for a vertical slice at the International Date Line. The perturbation is near 100% in the southern jet and >50% in the northern jet. The CO moves into the LMS via quasi-horizontal exchange, increasing CO by 25–100%.

#### 4.1.2 Slow ascent in the TTL

Figure 7a shows the CO perturbation in November near the tropical tropopause. The greatest perturbations (>100%) are over Africa, the Indian Ocean, and the region of the southern jet. Figure 7b shows the CO perturbations in the LS. The perturbations closely resemble those at the tropopause, first appearing over subtropical Asia, tropical Africa and the entire southern tropics in September and October. The maximum perturbations (~30 ppbv) occur in November over Africa and the tropical Indian Ocean, a region of preferential TST (Fueglistaler et al., 2004). At 60 mb (not shown), the CO perturbation (~5% or 1–2 ppbv) first appears over the tropical Atlantic and S. America in October; at this altitude, the total model CO is only 10–15 ppbv. By December, the perturbation is rather well-mixed, 10–25% (1–3 ppbv) and lingers through March.

The main entry point of the Indonesian pollution to the TTL does not occur over the Warm Pool. A number of factors conspire to minimize the impact of the pollution over the Pacific. First, much of the pollution disperses in the subtropical jets, which lay to the north and south of the Warm Pool. Second, most CO is transported to the Indian

Ocean because of a weak Walker Circulation and remains there because of weak and recirculating winds, as discussed above. Third, strong convection off the equatorial Pacific coast of Central America, which is associated with the strong El Niño, pumps air not significantly impacted by the wildfires from the lower troposphere to the UT (Fig. 5).

### 4.2 Impact on trace gases in the TTL and LS

The evolution of the monthly-averaged CO perturbation (%) in the TTL, LMS, and LS is shown in Fig. 8. The TTL perturbation peaks (50–60%) in October, the height of the fire activity, and remains >20% until January. There is a time lag of a month of the peak burden (>30%) in the LMS from that of the TTL and the perturbation remains >20% from October to January. The lag of the peak perturbation is two months for the LS as compared to the TTL.

An important feature in Fig. 8 is that the perturbation in the LMS is higher than in the LS, which implies that quasi-horizontal transport plays a more significant role in the TST of the pollution than slow ascent. However, we cannot quantify the significance as CO is not an inert tracer. For instance, the transit time of CO through slow ascent in the TTL, where OH is high, is several weeks. On the other hand, the lifetime is longer in the southern hemisphere (SH) subtropical jet region early in the study period as OH is low, but grows through austral spring as solar radiation increases. By November, the lifetimes near the tropical tropopause and the SH LMS are similar, 50–70 days. The reverse is true for the NH subtropical jet region, which explains why the NH portion, but not the SH portion, of the LMS perturbation remains high long after the fires end (Fig. 8).

The CO lifetime grows (as compared to the unperturbed case) because CO accumulates during the long burning event. OH is the primary sink for CO, so its zonal mean perturbation (Fig. 9a) closely follows that of the CO perturbation. In October, the OH perturbation in the TTL is negative (5–20%), especially in the region of the subtropical jets. When only the Indian Ocean region is considered, the OH in the entire TTL is

lower by >15% (Fig. 9b). While a 15% decrease in OH over several months in the TTL is significant by itself, it becomes even more important when one considers that air in the TTL typically resides there for several weeks before crossing the tropopause (Fueglislater et al., 2004). Therefore, a trace gas that has a primary sink by reaction with OH will have a longer lifetime, allowing more of it to cross the tropopause.

The zonal mean ozone perturbation is shown in Fig. 9c. It is >15% in much of the TTL from September to November and >25% (>15 ppbv) in October. When only the Indian Ocean is considered (Fig. 9d), the highest perturbation (>15 ppbv) in the TTL is along the equator and the southern subtropical jet, though the perturbation is >10 ppbv over the entire TTL. In a situation of enhanced ozone, the LZH will descend in altitude increasing the probability that air at this altitude will undergo TST, though this effect is not expected to be large for ozone (Gettelman et al., 2004). Nevertheless, this experiment shows that 1) biomass burning pollution can significantly elevate ozone in the entire TTL for many months, presumably impacting the dynamics there, and 2) ozone in both the LS and LMS can be impacted by a large biomass burning event.

## 5 Sources of variation in the TTL composition

In Sect. 4, we used an extreme biomass burning event, the 1997 Indonesian wildfires, to identify two main pathways for the pollution to enter the stratosphere: i. slow ascent in the TTL and ii. quasi-horizontal exchange in the regions of the subtropical jets. We find these two pathways are also important for more modest burning events. In Sect. 5, our goal is to understand how temporal and spatial variations in pollutant sources and dynamics impact the composition of the TTL and LMS. We examine the seasonal transport of biomass burning pollution to the UT/LS for a typical year, mid-1994 to mid-1995, to understand how usual variations in the timing and locations of burning contribute to CO perturbations in the TTL and LMS. We also investigate how the interannual variability of convection affects transport of pollutants to the TTL.

### 5.1 TST of regional biomass burning pollution

We performed five simulations. The base simulation is a standard simulation from mid-1994 to mid-1995 with climatological biomass burning sources. In the remaining simulations, we turned off sequentially the biomass burning emissions from four source regions: Africa south of the equator (86 Tg CO/y), Africa north of the equator (87 Tg CO/y), South America south of the equator (60 Tg CO/y), and Southeast Asia (82 Tg CO/y), not including Malaysia and Indonesia. Figure 10 shows the seasonal variation of biomass burning by region from 30° S–30° N.

#### 5.1.1 Southern hemisphere burning season

South America, southern Africa, and the tropical southern Atlantic Ocean experience widespread pollution during the SH burning season (Fishman et al., 1991; Thompson et al., 1996; Chatfield et al., 1998). Burning occurs in southern Africa typically from May to November and from August to November in South America (Fig. 10). The transport pathways from the two regions allow their plumes to inter-mingle. They can be treated as one plume for the purpose of this experiment.

The large biomass burning plume lies generally south of tropical easterlies and north of SH subtropical westerlies. Figure 11a shows that tropical easterlies play the dominant role, transporting much of the pollution to the Pacific Ocean. A broad area of convection extends from western Africa, across South America, and to the central Pacific, which lofts the pollution to the UT (Figs. 11b–c). By October, this pollution is being transported by the southern subtropical jet (Fig. 11c). Figure 11a also shows that subtropical westerlies transport surface pollution to the Indian Ocean; this pollution typically is not lofted to the UT as convection in the subtropics is not frequent.

Unlike the Indonesian pollution, ascent over the Warm Pool plays a role for pollution from South America and southern Africa. The pollution is first evident at the tropical tropopause in June over the Warm Pool and is >5% over much of the tropics by August (Fig. 11d). By November, the perturbation (~10–15%) becomes rather uniform.

The pollution reaches the LS in August and September along the equator from the central Pacific westward to Africa, though the perturbation is only 1–5% (not shown). It is widespread (>10%) in November and December, and >15% over central Africa in November. It reaches 60 mb by December, though it is generally ∼1–3% with the highest perturbation over the equatorial Pacific.

#### 5.1.2 Northern hemisphere burning season

*Northern Africa.* The burning season in northern Africa occurs mainly from November through March (Fig. 10). Much of the pollution near the surface moves with the tropical easterlies, polluting the entire tropical Atlantic and Pacific Oceans by February and March (not shown). A minor pathway to the western tropical Indian Ocean occurs during most of the burning season.

The Brewer-Dobson circulation is typically strongest in the NH winter when biomass burning peaks in northern Africa, and the northern subtropical jet is characterized by a strong potential vorticity gradient, creating a barrier to mixing (Chen, 1995). Therefore, one may expect that TST via slow ascent in the TTL would occur preferentially to exchange in the region of the northern subtropical jet. However, this is not the case as seasonal convection in central Africa provides the main transport pathway to the UT, especially in February and March when the ITCZ advances northward/closer to the burning regions. Consequently, the perturbation in the UT peaks in March and April (Fig. 12a), well into spring and several months after the peak in burning.

The perturbation near the tropical tropopause peaks from March to May (Fig. 12b), where it is >5% over the entire tropical tropopause region. However, it is first evident in January, when the highest values are 3–5% over Indonesia, the tropical Pacific, and South America. In the LS, the pollution first appears in January over the Warm Pool, and in February, it is >5% over two regions of deep convection, the Warm Pool and off the Pacific coast of Central America. It remains high (5–10%) from March through May over the entire tropics.

*Southeast Asia.* While the burning seasons occur over several months for the two

African regions and South America, approximately 50% of the biomass burned in Southeast Asia occurs in March (Fig. 10). Pollution is transported by the prevailing surface winds to the Indian and Pacific Oceans, where it is lofted to the UT by convection over the Bay of Bengal and the South China Sea. Figure 13a shows that the CO perturbation at 200 mb is >25% over the Bay of Bengal and Southeast Asia in March. This pollution is transported rapidly by the northern subtropical jet across the Pacific Ocean, circumnavigating the globe by April; the perturbation is 5–10% over much of the NH tropical and subtropical Indian and Pacific Oceans. A minor amount of the pollution is caught in the southern subtropical jet (Fig. 13a). The pollution first appears near the tropopause over the Warm Pool in February (~1%) and over large regions of the tropics by March and April (Fig. 13b). The pollution is high in April (>25%) over the Arabian Sea to the South China Sea and is >10% over most of the NH tropics and subtropics.

### 5.2 Contribution of sources

In Sect. 5.1, we showed the transport pathways of pollution from South America, southern Africa, northern Africa, and Southeast Asia to/within the UT/LS; these four regions account for 80% of the total biomass burning emissions (395 Tg CO/y) from 30° S–30° N. In our model, the mean CO in the tropical TTL (12° N–12° S) ranges between 44 and 58 ppbv for the 1994/95 burning season. Figure 14 shows the model's total CO (with the annual mean removed) and the CO perturbations in the TTL from the four source regions. Less than 20% of the total CO in the TTL is due to biomass burning. The perturbation from NH burning in boreal spring contributes more to the total CO in the TTL than SH burning in austral spring. The perturbation from northern Africa is higher than Southeast Asia, even though the emissions from both regions are similar. On the other hand, the CO perturbation from South America is higher, though emissions are ~30% lower, than from southern Africa; this occurs because convection is deeper over South America than southern Africa, especially in September. Together, the perturbations from the four regions explain about two-thirds of the seasonal vari-

ability in total CO in the TTL. That is, seasonal biomass burning drives the CO tape recorder, but other sources also contribute.

If biomass burning were the only source of seasonal variation, one would expect two maxima (during the NH and SH burning seasons) and two minima (the periods between them) in the mean CO each year in the TTL. This is not the case (Fig. 14). CO remains high during boreal winter, but not during austral winter. Figure 15 is the same as Fig. 14, except for the tropical LS (above 380 K and >60 mb; 12° N–12° S). Not surprisingly, the mean concentrations (16–25 ppbv) are lower than in the TTL and they peak 1–2 months later because of the transit time via slow ascent. The peak in total CO from SH burning in austral spring, as evident in the TTL (Fig. 14), is muted in the LS. These features are also seen in the observed tape recorder (Fig. 1 of Schoeberl et al., 2006).

Why does CO in the TTL remain high during boreal winter? First, the long-range transport of CO from fossil fuels and biofuels emitted in the NH extra-tropics and sub-tropics increases the background concentration of the northern tropics by ~20% in boreal winter/early spring (Duncan et al., 2007). (The time-scale of meridional transport is relatively long compared to the CO lifetime, except in winter when OH is low.) As this long-range transport occurs during the NH burning season, CO in the northern tropics reaches a seasonal maximum. Other CO sources (e.g., local fossil fuel and biofuel emissions, methane and NMHC oxidation) make much smaller or insignificant contributions to the seasonal variation of tropical CO (Duncan et al., 2007). Second, more CO crosses the tropopause in boreal winter as the ascent rate is higher than in boreal summer (Rosenlof, 1995); that is, a tape recorder would exist without seasonal changes in tropospheric CO sources.

The minimum in the CO tape recorder occurs in boreal summer in the TTL and late summer/early fall in the LS (Figs. 14–15). CO in the northern tropics is at an annual minimum as the NH burden of CO is seasonally low (Duncan et al., 2007). However, the Asian summer monsoon is active, lofting surface pollution from India (Fu et al., 2006). Indian emissions represent the largest source of CO from fossil fuel and biofuels year-

round in the tropics. MOPITT observations showed elevated CO in summer in the UT above India and China (Kar et al., 2004). At ~150 mb, elevated CO was observed in the MLS data over the Tibetan Plateau (Li et al., 2005). Consequently, one might expect Indian emissions during the monsoon to contribute significantly to the CO tape recorder. However, CO from India largely remains at latitudes >15° N, north of the TTL (12° N–12° S), as indicated by these observations. We find a similar result in a model simulation, in which we removed Indian emissions.

Pollution transported to the LMS does not contribute to the tape recorder. Figure 16 is the same as Fig. 14, except for the LMS of each hemisphere. The mean CO in the NH LMS ranges from 31–38 ppbv and from 21–25 ppbv in the SH LMS. As in the TTL and LS, most, but not all, of the variation is due to seasonal burning. CO from burning in each region pollutes the LMS of both hemispheres, but more so in the hemisphere in which burning occurs.

### 5.3 Interannual variability

In Sect. 4, we discussed the extreme burning event in Indonesia in 1997. The effects of El Niño are strongest typically during the SH burning season. Though, the ENSO-induced variability of precipitation is relatively weak year-round in southern Africa and South America. Consequently, the ENSO is not likely to be an important player in the IAV of biomass burning for these two regions. A similar argument can be made for burning in northern Africa and Southeast Asia, not including Indonesia. (The ENSO can impact the transport of pollution from these regions to the UT/LS (e.g., via locations and depths of convection) as discussed below.) In Sects. 5.1 and 5.2, we did not include simulations of biomass burning from Indonesia and Central America/Mexico as burning in these regions vary dramatically from year-to-year due to variations in ENSO. For instance, burning in Indonesia and Central America/Mexico during a La Niña is often 3–5 times less than during an El Niño (Duncan et al., 2003a); that is, historically only burning during an El Niño phase is of consequence.

Here, we discuss the dynamically-driven variability in the composition of the UT/LS

for five years, 1994–1998. Our simulations capture the IAV in meteorology associated with the phases of ENSO because the GCM was forced with observed SSTs. We use climatological biomass burning emissions for all five years.

Figure 17 shows the mean CO in the TTL for 1994–1998 with the 5-yr mean removed. The figure also shows the Oceanic Niño Index (ONI; degrees), where values >0.5°C indicate El Niño conditions and <–0.5°C indicate La Niña conditions. The El Niño phase occurred from April 1994 through March 1995 (i.e., the 1994/95 burning season), though from April through September the phase was relatively weak, and from May 1997 through April 1998 (i.e., the 1997/1998 burning season); this was one of the strongest El Niño events on record. The La Niña phase occurred from October 1995 through March 1996 (i.e., the 1995/96 burning season), though the entire phase was relatively weak. The other months, including the 1996/1997 burning season, were in the neutral phase (0.5°C>ONI>–0.5°C).

Clearly, the dynamics of the abnormally strong El Niño of 1997/1998 enhance transport to the TTL (Fig. 17). The CO perturbation in late 1997/early 1998 is the highest of the five years; this is the case in the LS as well (not shown). Figure 17 shows that the convective updraft flux in the model from 12° S–12° N is higher during the 1997/98 burning season as compared to the other years, which lofts more CO to the UT. Favorable dynamics, coupled with high emissions as discussed in Sect. 4, conspire to enhance the stratospheric impact of pollution from the catastrophic 1997/1998 burning season.

Minus the unusual El Niño of 1997/1998, there is significant IAV between the years in total CO. For instance, the minimum CO occurs in July and August in 1995, 1996, and 1998, during neutral or La Niña conditions; the two years with the highest minimums occur in 1994 and 1997 during El Niño events. In the SH burning season, the highest CO occurs in 1997 and 1998, two extreme phases of ENSO. We also analyzed IAV of the CO perturbation in the TTL by region. We find that IAV in the frequency, depth, and location of deep convection causes variations in CO in the UT. For instance, the CO perturbation from Southeast Asia in the TTL is 25% higher in 1994 than either 1995 or

1996.

## 6 Conclusions

The CO tape recorder in the MLS data showed that biomass burning pollution is transported regularly to the LS. In this study, we investigated the cross-tropopause transport of the pollution and assessed the impact on the composition and chemistry of the UT/LS. Strahan et al. (2007) used a variety of satellite and aircraft-derived transport diagnostics to show that the GMI COMBO CTM reproduces observations reasonably well in the UT/LS, which lends confidence in its use as a tool to study the TST of pollution.

We found that the two pathways of TST, slow ascent in the TTL and quasi-horizontal exchange in the region of the subtropical jets, are of similar importance. However, the latter pathway delivers the pollution to the LMS, where it most likely returns to the troposphere (Schoeberl et al., 2004); most tropical biomass burning occurs in local spring, a season of strong stratosphere-to-troposphere transport in the extra-tropics, associated with the Brewer-Dobson circulation. In general, the relative importance of the two TST pathways depends on the lifetime of a trace gas, which is typically longer in the region of the subtropical jets than the TTL where solar radiation and OH are consistently higher.

We performed a simulation of one of the largest burning events of the 20th century, the 1997 Indonesian wildfires, to provide an upper bound on the impact of biomass burning on the UT/LS. The fires occurred during the SH burning season, so that the total emissions were about twice that of the Indonesian fires alone. For perspective, the burning emissions of CO equaled almost 70% of annual, global fossil fuel emissions.

The main entry point of the Indonesian pollution to the UT/LS occurred over the Indian Ocean and Africa, and not the Warm Pool, because of a weak Walker Circulation (i.e., the pollution moved to the Indian Ocean, not the Pacific). Weak and recirculating winds largely confined the pollution to the Indian Ocean, except for the subtropical

jets which transported the pollution north and south of the Warm Pool. The Walker Circulation is historically weak during El Niños, so it is possible that pollution from widespread wildfires in Indonesia (e.g., 1982–1983, 1991, 1994, 1997–1998) followed similar transport pathways as in 1997.

During this burning event, both ozone and CO associated with the fires contributed to their burdens in the UT/LS, which lasted well after the fires ended. For instance, ozone was 5–20% higher on average in the TTL and >100% over parts of the Indian Ocean for several months. The increased CO lengthened the lifetimes of trace gases, including itself, as reaction with CO is the primary sink for OH, which was 5–20% lower in most of the TTL. The lower OH allowed higher amounts of trace gases to cross the tropopause for several months.

In addition to the Indonesian fires, we assessed the transport pathways and impact of pollution of more typical burning from four regions: southern Africa, northern Africa, Southeast Asia, and South America. With these experiments, we showed that pollution is transported regularly to the TTL/LS, impacting the composition of trace gases there. In general, the peaks in burning in South America and southern Africa occur at the same time in austral spring. We found that much of the pollution from South America and southern Africa mixes and follows similar transport pathways in the UT/LS, entering the LS via slow ascent over the Warm Pool and Africa, both regions of preferential TST. As with the Indonesian pollution, quasi-horizontal exchange in the region of the subtropical jets is important. For the NH season, peak burning in northern Africa and Southeast Asia (i.e., Indochina) are offset by several months. Nevertheless, the transport pathways to the UT/LS are similar for these two regions as for southern Africa and South America. These four regions contribute equally to the seasonal variation in the TTL.

We found that seasonal variation of CO in the TTL/LS results predominately from seasonal biomass burning, but that the long-range transport of CO from the subtropics and mid-latitudes of the NH in boreal winter also plays a role. This partially explains why CO in the TTL in boreal winter (between the SH and NH burning seasons) is higher



ACPD
7, 2197–2248, 2007

than in austral winter (between the NH and SH burning seasons). In the LS, there is only one minimum in CO in the latter half of the year and one maximum in the beginning of the year. That is, the minimum between the SH and NH burning seasons disappears as slow ascent in the TTL is seasonally faster in boreal winter than summer (Rosenlof, 1995).

We conclude that there are two main sources of interannual variation in CO in the TTL/LS for our study period, 1994–1998. First, year-to-year changes in the locations, frequencies, and depths of deep convection loft varying amounts of biomass burning CO to the UT. The highest concentrations in the TTL occurred during the 1997/98 El Niño event because of stronger convective transport to the UT during this time. Second, year-to-year changes in biomass burning are substantial, especially high during El Niño years when large wildfires typically occur in Indonesia and Central America.

We could not assess the impact of the changes in atmospheric composition (e.g., ozone, water vapor) on the dynamics of the TTL/LS as we used a CTM. For example, what were the impacts of the fire's aerosols on clouds and, subsequently, on radiation in the LS? Another potentially important impact is that the sizable amount of aerosols emitted by the Indonesian wildfires (Duncan et al., 2003b) could have decreased the average size of ice crystals, allowing more water vapor to enter the stratosphere (Sherwood, 2002). Therefore, as future work, we plan to conduct sensitivity studies with a general circulation model to understand the impact of biomass burning pollution on ascent in the TTL.

*Acknowledgements.* We would like to thank J. Rodriguez and the GMI core modeling team for their efforts which have facilitated our research. We wish to thank E. Nielsen of NASA GMAO for providing us with meteorological fields. We thank A. Douglass and M. Schoeberl for their scientific insight and advice. We gratefully acknowledge those who provided us with their observational data. The Japan Airlines data were provided by H. Matsueda of the Geochemical Research Department, Meteorological Research Institute, Japan. The surface CO data were provided by NOAA GMD. Aircraft measurements were provided by the MOZAIC program (http://www.aero.obs-mip.fr/mozaic). The GPCP combined precipitation data were developed and computed by the NASA/Goddard Space Flight Center's Laboratory for Atmospheres as a

contribution to the GEWEX Global Precipitation Climatology Project. This research was supported by NASA Grant MAP/04-0068-0040.

## References

Adler, R. F., Huffman, G. J. Chang, A., Ferraro, R., Xie, P., Janowiak, J., Rudolf, B., Schneider, U., Curtis, S., Bolvin, D., Gruber, A., Susskind, J., and Arkin, P.: The Version 2 Global Precipitation Climatology Project (GPCP) Monthly Precipitation Analysis (1979–Present), J. Hydrometeorol., 4(6), 1147–1167, 2003.

Andreae, M. and Merlet, P.: Emission of trace gases and aerosols from biomass burning, Global Biogeochemical Cycles, 15, 955–966, 2001.

Baughcum, S. L., Tritz, T. G., Hernerdon, S. C., and Pickett, D. C.: Scheduled civil aircraft emission inventories for 1992: database development and analysis, NASA CR-4700, Natl. Aeronaut and Space Admin., Washington, D.C., 1996.

Benkovitz, C. M., Scholtz, M. T., Pacyna, J., Tarrason, L., Dignon, J., Voldner, E. C., Spiro, P. A., Logan, J. A., and Graedel, T. E.: Global gridded inventories of anthropogenic emissions of sulfur and nitrogen, J. Geophys. Res., 101, 29 239–29 253, 1996.

Bey, I., Jacob, D. J., Yantosca, R. M., Logan, J. A., Field, B. D., Fiore, A. M., Li, Q., Liu, H., Mickley, L. J., and Schultz, M.: Global modeling of tropospheric chemistry with assimilated meteorology: Model description and evaluation, J. Geophys. Res., 106, 23 073–23 095, 2001.

Bian, H. and Prather, M. J.: Fast-J2: Accurate Simulation of stratospheric photolysis in global chemical models, J. Atmos. Chem., 41, 281–296, 2002.

Bloom, S., da Silva, A., Dee, D., Bosilovich, M., Chern, J.-D., Pawson, S., Schubert, S., Sienkiewicz, M., Stajner, I., Tan, W.-W., and Wu, M.-L.: Documentation and validation of the Goddard Earth Observing System (GEOS) Data Assimilation System – Version 4, Technical Report Series on Global Modeling and Data Assimilation 104606, 2005.

Chatfield, R. B., Vastano, J. A., Li, L., Sachse, G. W., and Connors, V. S., The Great African plume from biomass burning: Generalizations from a three-dimensional study of TRACE A carbon monoxide, J. Geophys. Res. 103, 28 059–28 077, 1998.

Chatfield, R. B., Guo, Z., Sachse, G. W., Blake, D. R., and Blake, N. J.: The subtropical global plume in the Pacific Exploratory Mission-Tropics A (PEM-Tropics A), PEM-Tropics B, and the

Global Atmospheric Sampling Program (GASP): How tropical emissions affect the remote Pacific, J. Geophys. Res., 107, 4278, doi:10.1029/2001JD000497, 2002.
Chin, M., Ginoux, P., Kinne, S., Torres, O., Holben, B., Duncan, B., Martin, R., Logan, J., Higurashi, A., and Nakajima. T.: Tropospheric aerosol optical thickness from the GOCART model and comparisons with satellite and sunphotometer measurements, J. Atmos. Sci., 59, 461–483, 2002.
Considine, D. B., Douglass, A. R., Connell, P. S., Kinnison, D. E., and Rotman, D. A.: A polar stratospheric cloud parameterization for the three-dimensional model of the global modeling initiative and its response to stratospheric aircraft, J. Geophys. Res., 105, 3955–3975, 2000.
Dai, A. and Wigley, T. M. L.: Global patterns of ENSO-induced precipitation, Geophys. Res. Lett., 27, 1283–1286, 2000.
de Laat, A. T. J., Aben, I., and Roelofs, G. J.: A model perspective on total tropospheric $O_3$ column variability and implications for satellite observations, J. Geophys. Res., 110, D13303, doi:10.1029/2004JD005264, 2005.
Dessler, A. E.: A reexamination of the "stratospheric fountain" hypothesis, Geophys. Res. Lett., 25, 4165–4168, 1998.
Dethof, A., O'Neill, A., Slingo, J. M., and Smit H. G. J.: A mechanism for moistening the lower stratosphere involving the Asian summer monsoon, Q. J. R. Meteorol. Soc., 125, 1079–1106, Part B., 1999.
Douglass, A. R., Schoeberl, M. R., Rood, R. B., and Pawson, S.: Evaluation of transport in the lower tropical stratosphere in a global chemistry and transport model, J. Geophys. Res., 108(D9), 4259, doi:10.1029/2002JD002696, 2003.
Douglass, A. R., Stolarski, R. S., Strahan, S. E., and Connell, P. S.: Radicals and reservoirs in the GMI chemistry and transport model: Comparison to measurements, J. Geophys. Res., D16302, doi:10.1029/2004JD004632, 2004.
Dlugokencky , E. J., Masarie, K. A., Lang, P. M., and Tans, P. P.: Continuing decline in the growth rate of the atmospheric methane burden, Nature, 393, 447–450, 1998.
Duncan, B. N., Martin, R., Staudt, A., Yevich, R., and Logan, J.: Interannual and Seasonal Variability of Biomass Burning Emissions Constrained by Satellite Observations, J. Geophys. Res., 108, 4100, doi:10.1029/2002JD002378, 2003a.
Duncan, B. N., Bey, I., Chin, M., Mickley, L. J., Fairlie, T. D., Martin, R. V., and Matsueda, H.: Indonesian Wildfires of 1997: Impact on Tropospheric Chemistry, J. Geophys. Res., 108, 4458, doi:10.1029/2002JD003195, 2003b.

Dunlea, E. J. and Ravishankara, A. R.: Kinetic studies of the reactions of O(1D) with several atmospheric molecules, Phys. Chem. Chem. Phys., 6, doi:10.1039/b400247d, 2004.
Evans, M. J, and Jacob, D. J.: Impact of new laboratory studies of $N_2O_5$ hydrolysis on global model budgets of tropospheric nitrogen oxides, ozone, and OH, Geophys. Res. Lett., 32, L09813, doi:10.1029/2005GL022469, 2005.
Fishman, J., Fakruzzaman, F., Cros, B., and Nganga, D.: Identification of widespread pollution in the Southern Hemisphere deduced from satellite analyses, Science, 252, 1693–1696, 1991.
Folkins, I., Chatfield, R., Baumgardner, D., and Proffitt, M.: Biomass burning and deep convection in southeastern Asia: Results from ASHOE/MAESA, J. Geophys. Res., 102, 13 291–13 299, 1997.
Folkins, I., Loewenstein, M., Podolske, J., Oltmans, S. J., and Proffitt, M.: A barrier to vertical mixing at 14 km in the tropics: Evidence from ozonesondes and aircraft measurements, J. Geophys. Res., 104, 22 095–22 102, 1999.
Folkins, I., Bernath, P., Boone, C., Lesins, G., Livesay, N., Thompson, A. M., Walker, K., and Witte, J. C.: The seasonal cycles of $O_3$, CO, and convective outflow at the tropical tropopause, Geophys. Res. Lett., 33, L16802, doi:10.1029/2006GL026602, 2006.
Fromm, M., Bevilacqua, R., Servranckx, R., Rosen, J., Thayer, J., Herman, J., and Larko, D.: Pyro-cumulonimbus injection of smoke to the stratosphere: Observations and impact of a super blowup in northwestern Canada on 3–4 August 1998, J. Geophys. Res., 110, D08205, doi:10.1029/2004JD005350, 2005.
Fueglistaler, S., Wernli, H., and Peter, T.: Tropical troposphere-to-stratosphere transport inferred from trajectory calculations, J. Geophys. Res., 109, D03108, doi:10.1029/2003JD004069, 2004.
Fueglistaler, S. and Fu, Q.: Impact of clouds on radiative heating rates in the tropical lower stratosphere, J. Geophys. Res., 111, D23202, doi:10.1029/2006JD007273, 2006.
Fu, R., Y. Hu, Wright, J. S., Jiang, J. H., Dickinson, R. E., Chen, M., Filipiak, M., Read, W. G., Waters, J. W., and Wu, D. L.: Short-circuit of water vapor and polluted air to the global stratosphere by convective transport over the Tibetan Plateau, PNAS, doi:10.1073/pnas.0601584103, 2006.
Garstang, M., Tyson, P. D., Swap, R., Edwards, M., Kållberg, P., and Lindesay, J. A.: Horizontal and vertical transport of air over southern Africa, J. Geophys. Res., 101, 23 721–23 736, 1996.

Gettelman, A., de F. Forster, P. M., Fujiwara, M., Fu, Q., Vömel, H., Gohar, L. K., Johanson, C., and Ammerman, M.: Radiation balance of the tropical tropopause layer, J. Geophys. Res., 109, D07103, doi:10.1029/2003JD004190, 2004.
Guenther, A., Hewitt, C. N., Erickson, D., et al.: A global model of natural volatile organic compound emissions, J. Geophys. Res., 100, 8873–8892, 1995.
Hack, J. J.: Parameterization of moist convection in the NCAR Community Climate Model, CCM2, J. Geophys. Res., 99, 5551–5568, 1994.
Holton, J. R., Haynes, P. H., McIntyre, M. E., Douglass, A. R., Rood, R. B., and Pfister, L.: Stratosphere-Troposphere Exchange, Rev. Geophys., 33, 403–439, 1995.
Jacobson, M. Z.: Computation of global photochemistry with SMVGEAR II, Atmos. Environ., 29, 2541–2546, 1995.
Jacob, D. and Bakwin, P.: Cycling of $NO_x$ in tropical forest canopies and its implications for the global source of biogenic $NO_x$ to the atmosphere, in Microbial Production and Consumption of Greenhouse Gases, edited by: Whitman, W. B., American Society of Microbiology, Washingoton, D.C., 1991.
Jacob, D. J., Field, B. D., Jin, E., Bey, I., Li, Q. B., Logan, J. A., and Yantosca, R. M.: Atmospheric budget of acetone, J. Geophys. Res., 107, 4100, doi:10.1029/2001JD000694, 2002.
Jacob, D. J., Crawford, J. H., Kleb, M. M., et al.: Transport and chemical evolution over the Pacific (TRACE-P) aircraft mission: Design, execution, and first results, J. Geophys. Res., 108, 9000, doi:10.1029/2002JD003276, 2003.
Kar, J., Bremer, H., Drummond, J. R., et al.: Evidence of vertical transport of carbon monoxide from Measurements of Pollution in the Troposphere (MOPITT), Geophys. Res. Lett., L23105, doi:10.1029/2004GL021128, 2004.
Kar, J., Drummond, J. R., Jones, D. B. A., Liu, J., Nichitiu, F., Zou, J., Gille, J. C., Edwards, D. P., and Deeter, M. N.: Carbon monoxide (CO) maximum over the Zagros mountains in the Middle East: Signature of mountain venting?, Geophys. Res. Lett., 33, L15819, doi:10.1029/2006GL026231, 2006.
Kinnison, D. E., Connell, P. S., Rodriguez, J. M., Rotman, D. A., Considine, D. B., Tannahil, J., Ramaroson, R., Rasch, P. J., Douglass, A. R., Baughcum, S. L., Coy, L., Waugh, D. W., Kawa, S. R., and Prather, M. J.: The Global Modeling Initiative Assessment Model: Application to High-Speed Civil Transport Perturbation, J. Geophys. Res., 106, 1693–1712, 2001.
Kley, D., Crutzen, P. J., Smit, H. G. J., Vömel, H., Oltmans, S. J., Grassl, H., and Ramanathan,

V.: Observations of near-zero ozone concentrations over the convective Pacific: Effects on air chemistry, Science, 274, 230–232, 1996.

Li, Q., Jiang, J. H., Wu, D. L., et al: Convective outflow of South Asian pollution: A global CTM simulation compared with EOS MLS observations, Geophys. Res. Lett., L14826, doi:10.1029/2005GL022762, 2005.

Lin, S.-J. and Rood, R. B.: Multidimensional flux-form semiLagrangian transport schemes, Mon. Weather Rev., 124, 2046–2070, 1996.

Liu, H., Jacob, D. J., Bey, I., and Yantosca, R. M.: Constraints from $^{210}$Pb and $^{7}$Be on wet deposition and transport in a global three-dimensional chemical tracer model driven by assimilated meteorological fields, J. Geophys. Res., 106, 12 109–12 128, 2001.

Liu, C. and Zipser, E. J.: Global distribution of convection penetrating the tropical tropopause, J. Geophys. Res., 110, doi:10.10292005JD006063, 2005.

Livesey, N. J., Fromm, M. D., Waters, J. W., Manney, G. L., Santee, M. L., and Read, W. G.: Enhancements in lower stratospheric $CH_3CN$ observed by the Upper Atmosphere Research Satellite Microwave Limb Sounder following boreal forest fires, J. Geophys. Res., 109, D06308, doi:10.1029/2003JD004055, 2004.

Metwally, M.: Jet aircraft engine emissions database development: 1992 military, charter and nonscheduled traffic, NASA CR-4684, Natl. Aeronaut. and Space Admin., Washington, D.C., 1995.

Martin, R. V., Jacob, D. J., Yantosca, R. M., et al.: Global and regional decreases in tropospheric oxidants from photochemical effects of aerosols, J. Geophys. Res., 108(D3), 4097, doi:10.1029/2002JD002622, 2003.

Matsueda, H., Inoue, H. Y., Sawa, Y.,Tsutsumi, Y., and Ishii, M.: Carbon monoxide in the upper troposphere over the western Pacific between 1993 and 1996 J. Geophys. Res., 103, 19 093–19 110, 1998.

Matsueda, H. and Inoue, H. Y.: Aircraft measurements of trace gases between Japan and Singapore in October of 1993, 1996, and 1997, Geophys. Res. Lett., 26, 2413–2416, 1999.

Matsueda, H., Inoue, H. Y., Ishii, M., and Tsutsumi, Y.: Large injection of carbon monoxide into the upper troposphere due to intense biomass burning in 1997, J. Geophys. Res., 104, 26 867–26 879, 1999.

Mote, P. W., Rosenlof, K. H., McIntyre, M. E., et al.: An atmospheric tape recorder: The imprint of tropical tropopause temperatures on stratospheric water vapor, J. Geophys. Res., 101, 3989–4006, 1996.

Newell, R. E. and Gould-Stewart, S.: A Stratospheric Fountain?, Am. Meteorol. Soc., 38, 2789–2796, 1981.
Novelli, P. C., Steele, L. P., and Tans, P. P.: Mixing ratios of carbon monoxide in the troposphere, J. Geophys. Res., 102, 12 855–12 861, 1992.
Novelli, P. C., Masarie, K. A., and Lang, P. M.: Distributions and recent changes in carbon monoxide in the lower troposphere, J. Geophys. Res., 103, 19 015–19 033, 1998.
Olivier, J. G. J., Pieter, J., Bloos, J., Berdowski, J. J. M., Visschedijk, A. J. H. and Bouwman, A. F.: A 1990 global emission inventory of anthropogenic sources of carbon monoxide on 1°×1° developed in the framework of EDGAR/GEIA, Chemosphere: Global Change Sci., 1, 1–17, 1999.
Olivier, J. G. J., Berdowski, J. J. M., Peters, J. A. H. W., Bakker, J., Visschedijk, A. J. H., and Bloos, J.-P. J.: Applications of EDGAR. Including a description of EDGAR 3.0: reference database with trend data for 1970–1995. RIVM, Bilthoven. RIVM report no. 773301 001/ NOP report no. 410200 051, 2001.
Olson, J.: World ecosystems (WE1.4): Digital raster data on a 10 minute geographic 1080 x 2160 grid, in Global ecosystems database, version 1.0: Disc A, Ed. NOAA Natl. Geophys. Data Center, Boulder, CO, 1992.
Piccot, S., Watson, J., and Jones, J.: A global inventory of volatile organic compound emissions from anthropogenic sources, J. Geophys. Res., 97, 9897–9912, 1992.
Price, C. and Rind, D.: A simple lightning parameterization for calculating global lightning distributions, J. Geophys. Res., 97, 9919–9933, 1992.
Price, C., Penner, J., and Prather, M.: $NO_x$ from lightning, Part I: Global distribution based on lightning physics, J. Geophys. Res., 102, 5929–5941, 1997.
Pickering, K. E., Wang, Y. S., Tao, W. K., Price, C., and Muller, J. F.: Convective transport of biomass burning emissions over Brazil during TRACE A, J. Geophys. Res., 101, 23 993–24 012, 1996.
Pickering, K. E., Wang, Y. S., Tao, W. K., Price, C., and Muller, J. F.: Vertical distributions of lightning $NO_x$ for use in regional and global chemical transport models, J. Geophys. Res., 103(D23), 31 203–31 216, 1998.
Prinn, R. G., Huang, J., Weiss, R. F., et al.: Evidence for variability of atmospheric hydroxyl radicals over the past quarter century, Geophys. Res. Lett., 32, L07809, doi:10.1029/2004GL022228, 2005.
Randel, W. J. III, Zawodny, J. M., and Oltmans, S. J.: Seasonal variation of water vapor in

the lower stratosphere observed in Halogen Occultation Experiment data, J. Geophys. Res., 106, 14 313–14 325, 2001.
Rasch, P. J., Mahowald, N. M., and Eaton, B. E.: Representations of transport, convection, and the hydrologic cycle in chemical transport models: Implications for the modeling of short-lived and soluble species, J. Geophys. Res., 102, 28 127–28 138, 1997.
Rosenlof, K. H.: Seasonal cycle of the residual mean meridional circulation in the stratosphere, J. Geophys. Res., 100, 5173–5191, 1995.
Rotman, D. A., Tannahill, J. R., Kinnison, D. E., Connell, P. S., Bergmann, D., Proctor, D., Rodriguez, J. M., Lin, S. J., Rood, R. B., Prather, M. J., Rasch, P. J., Considine, D. B., Ramaroson, R., and Kawa, S. R.: Global Modeling Initiative assessment model: Model description, integration, and testing of the transport shell, J. Geophys. Res., 106, 1669–1691, 2001.
Schoeberl, M. R., Douglass, A. R., Zhu, Z., and Pawson, S.: A comparison of the lower stratospheric age spectra derived from a general circulation model and two data assimilation systems, J. Geophys. Res., 108(D3), 4113, doi:10.1029/2002JD002652, 2003.
Schoeberl, M. R., Douglass, A. R., Hilsenrath, E., et al.: Earth observing systems benefit atmospheric research, EOS, 85, 177–178, 2004.
Schoeberl, M. R., Duncan, B. N., Douglass, A. R., Waters, J., Livesey, N., Read, W., and Filipiak, M.: The carbon monoxide tape recorder, Geophys. Res. Lett., 33, L12811, doi:10.1029/2006GL026178, 2006.
Sherwood, S. C.: A stratospheric "drain" over the Maritime Continent, Geophys. Res. Lett., 27, 677–680, 2000.
Sherwood, S. C.: A microphysical connection among biomass burning cumulus clouds, and stratospheric moisture, Science, 295, 1272–1275, 2002.
Spivakovsky, C. M., Logan, J. A., Montzka, S. A., et al.: Three-dimensional climatological distribution of tropospheric OH: Update and evaluation, J. Geophys. Res., 105, 8931–8980, 2000.
Staudt, A. C., Jacob, D. J., Logan, J. A., Bachiochi, D., Krishnamurti, T. N., and Poisson, N.: Global chemical model analysis of biomass burning and lightning influences over the South Pacific in austral spring, J. Geophys. Res., 107, 4200, doi:10.1029/2000JD000296, 2002.
Strahan, S. E., Duncan, B. N., and Hoor, P.: Observationally derived transport diagnostics for the lowermost stratosphere and their application to the GMI chemistry and transport model, Atmos. Chem. and Phys. Discuss., 7, 1449–1477, 2007.

Thompson, A. M., Pickering, K. E., McNamara, D. P., Schoeberl, M. R., Hudson, R. D., Kim, J. H., Browell, E. V., Kirchoff, V. W. J. H., and Nganga, D.: Where did tropospheric ozone over southern Africa and the tropical Atlantic come from in October 1992? Insights from TOMS, GTE TRACE A, and SAFARI 1992, J. Geophys. Res., 101, 24 251–24 278, 1996.

van der Werf, G., Anderson, J., Giglio, L., Collatz, G., and Kashibhatla, P.: Interannual variability in global biomass burning emissions from 1997 to 2004, Atmos. Chem. and Phys., 6, 3423–3441, 2006.

Wang, Y., Jacob, D. J., and Logan, J. A.: Global simulation of tropospheric $O_3$-$NO_x$-hydrocarbon chemistry: 1. Model formulation, J. Geophys. Res., 103, 10 713–10 725, 1998.

Wesely, M., Cook, D. R., Hart, R. L., and Speer, R. E.: Measurements and parameterization of particulate sulfur dry deposition over grass, J. Geophys. Res., 90, 2131–2143, 1985.

Wild, O., Zhu, X., and Prather, M. J.: Fast-J: Accurate simulation of in- and below-cloud photolysis in tropospheric chemical models, J. Atmos. Chem., 37, 245–282, 2000.

Yevich, R. and Logan, J. A.: An assessment of biofuel use and burning of agricultural waste in the developing world, Global Biogeochem. Cycles, 17 (4), 1095, doi:10.1029/2002GB001952, 2003.

Zhang, G. J. and McFarlane, N. A.: Sensitivity of climate simulations to the parameterization of cumulus convection in the Canadian Climate Centre general circulation model, Atmos. Ocean, 33, 407–446, 1995.

Ziemke, J.R., Chandra, S., Duncan, B. N., Froidevaux, L., Bhartia, P. K., Levelt, P. F., and Waters, J. W.: Tropospheric ozone determined from Aura OMI and MLS: Evaluation of measurements and comparison with the Global Modeling Initiative's Chemical Transport Model, J. Geophys. Res., 111, D19303, doi:10.1029/2006JD007089, 2006.

**Table 1.** Annual Emissions in the COMBO CTM.

| Source | $NO_x$ Tg N | CO Tg direct | CO Tg indirect | MEK Tg C | PRPE Tg C | $C_2H_6$ Tg C | $C_3H_8$ Tg C | ALK4 Tg C | ALD2 Tg C | $CH_2O$ Tg C | ISOP Tg C | NMHC Tg C |
|---|---|---|---|---|---|---|---|---|---|---|---|---|
| Soils | 6.6 | – | | – | – | – | – | – | – | – | – | – |
| Vegetation | – | – | 150.5[a] | – | 10.9 | – | – | – | – | – | 380.0 | 390.9 |
| Aircraft[b] | 0.6 | – | | – | – | – | – | – | – | – | – | – |
| Lightning[c] | 5.0 | – | | – | – | – | – | – | – | – | – | – |
| Fossil Fuel[b] | 23.6 | 393.8[d] | 7.9[e] | 0.8 | 7.9 | 5.3 | 5.7 | 25.2 | – | – | – | 44.9 |
| Biomass[c] | 6.5 | 439.3 | 22.0[e] | 3.6 | 3.9 | 1.9 | 0.7 | 0.6 | 2.6 | 1.9 | – | 15.3 |
| Biofuel[b] | 2.2 | 160.3 | 13.8[e] | 1.3 | 6.3 | 2.0 | 0.9 | 0.8 | 0.7 | 0.5 | – | 12.4 |
| Total | 44.5 | 993.4 | 194.2 | 5.8 | 29.0 | 9.3 | 7.3 | 26.6 | 3.3 | 2.4 | 380.0 | 463.5 |

[a] Emissions from the oxidation of 1) biogenic methanol (100 Tg CO) and 2) monoterpenes (50.5 Tg CO). [b] Annual mean emissions. [c] Monthly mean emissions. [d] Scaled 10% higher in summer and 10% lower in winter. [e] CO derived from photochemical oxidation of NMHC not accounted for in anthropogenic NMHC emission inventory. PRPE = lumped $\geq C_3$ alkenes; ALK4 = lumped $\geq C_4$ alkanes; ALD2 = acetaldehyde; ISOP = isoprene.

**Table 2.** Statistical Comparison of the Model with GMD Observations (1994–1998).

| Station ID | Station Location | Lat deg | Lon deg | Alt m | N [a] | Δ[b] ppbv | Δ[c] % | Std. Err.[d] ppbv | R[2e] |
|---|---|---|---|---|---|---|---|---|---|
| *High N. Hemisphere* | | | | | | | | | |
| ALT | Alert, Canada | 82° N | 62° W | 210 | 60 | –18 | –10 | 2.5 | 0.78 |
| MBC | Mould Bay, Canada | 76° N | 119° W | 58 | 41 | –17 | –10 | 2.5 | 0.88 |
| BRW | Barrow, Alaska | 71° N | 36° W | 11 | 60 | –19 | –10 | 2.7 | 0.76 |
| ICE | Heimaey, Iceland | 63° N | 20° W | 100 | 60 | –15 | –9.4 | 2.0 | 0.73 |
| *Europe* | | | | | | | | | |
| MHD | Mace Head, Ireland | 53° N | 9° W | 25 | 60 | –12 | –7.6 | 2.2 | 0.56 |
| HUN | Hegyhatsal, Hungary | 46° N | 16° E | 248 | 60 | –40 | –15 | 5.3 | 0.47 |
| *N. America & N. Atlantic* | | | | | | | | | |
| CMO | Cape Meares, Oregon | 45° N | 123° W | 30 | 51 | –18 | –9.4 | 3.1 | 0.66 |
| NWR | Niwot Ridge, Colorado | 40° N | 105° W | 3475 | 60 | –15 | –10 | 2.2 | 0.28 |
| ITN | Grifton, North Carolina | 35° N | 77° W | 505 | 60 | –8.8 | –3.1 | 3.9 | 0.18 |
| BMW | Southhampton, Bermuda | 32° N | 65° W | 30 | 60 | –24 | –18 | 1.9 | 0.75 |
| IZO | Tenerife, Canary Islands | 28° N | 16° W | 2300 | 60 | –15 | –10 | 2.6 | 0.34 |
| RPB | Ragged Pt., Barbados | 13° N | 59° W | 3 | 60 | –12 | –12 | 1.4 | 0.54 |
| *E. Asia & N. Pacific* | | | | | | | | | |
| CBA | Cold_Bay, Alaska | 55° N | 162° W | 25 | 60 | –17 | –10 | 2.3 | 0.76 |
| TAP | Tae-ahn, S. Korea | 36° N | 126° E | 20 | 60 | –17 | –5.3 | 6.0 | 0.09 |
| WLG | Mt. Waliguan, PRC | 36° N | 100° E | 3810 | 60 | –12 | –6.9 | 3.6 | 0.02 |
| MID | Sand Island, Midway | 28N | 177° W | 4 | 60 | –31 | –24 | 1.8 | 0.85 |
| MLO | Mauna Loa, Hawaii | 19° N | 155° W | 3397 | 60 | –20 | –20 | 1.6 | 0.67 |
| GMI | Guam, Mariana Islands | 13° N | 144° E | 2 | 60 | –22 | –22 | 1.4 | 0.77 |
| *S. Hemisphere Tropics* | | | | | | | | | |
| SEY | Mahe Island, Seychelles | 4° S | 55° E | 3 | 56 | –26 | –28 | 2.5 | 0.38 |
| ASC | Ascension Island | 7° S | 14° W | 54 | 60 | –12 | –14 | 1.7 | 0.29 |
| SMO | American Samoa | 14° S | 170° W | 42 | 60 | –7.9 | –12 | 1.2 | 0.01 |
| *Mid & High S. Hemisphere* | | | | | | | | | |
| EIC | Easter Island | 27° S | 109° W | 50 | 59 | –14 | –23 | 0.8 | 0.60 |
| CGO | Cape Grim, Tasmania | 40° S | 144° E | 94 | 60 | –2.5 | –3.0 | 0.9 | 0.36 |
| SYO | Syowa, Antarctica | 69° S | 39° E | 11 | 60 | –7.9 | –16 | 0.6 | 0.74 |

[a] N is the number of monthly mean observations coincident with the model output; [b] The bias is the mean of (model-observed)/observed for the entire time series; [c] Mean bias (%) relative to the mean observed CO; [d] Standard error of mean bias (Δ); [e] R is the linear correlation coefficient between model and observations.

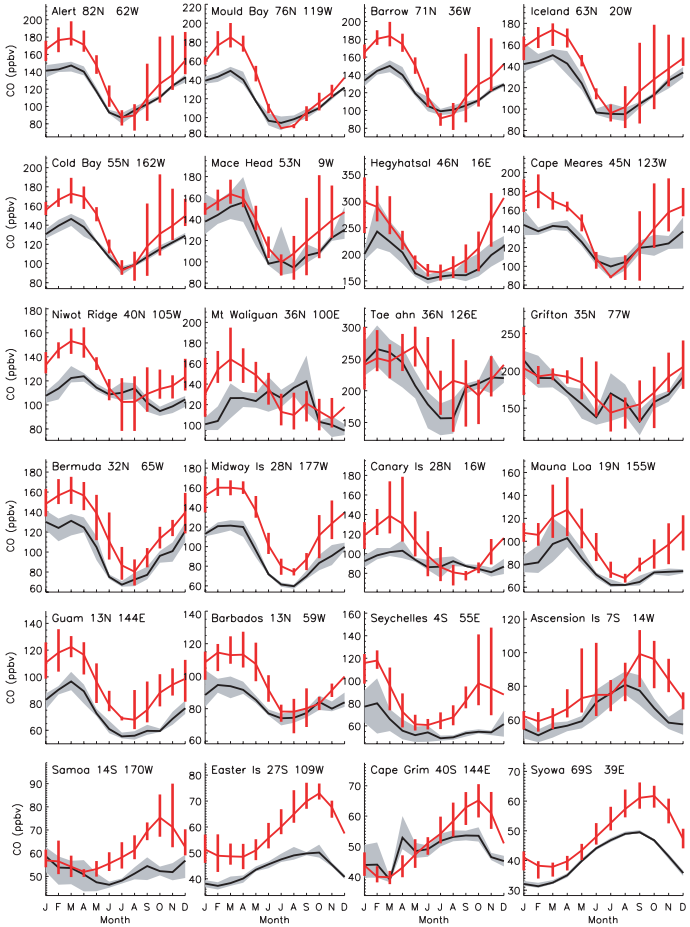


**Fig. 1.** Comparison of mean (1994–1998) CO from the model (black line) and GMD observations (red line). The red vertical bars and gray shaded area show the range of the observations and model, respectively. Station locations are shown in Table 2.



ACPD
7, 2197–2248, 2007

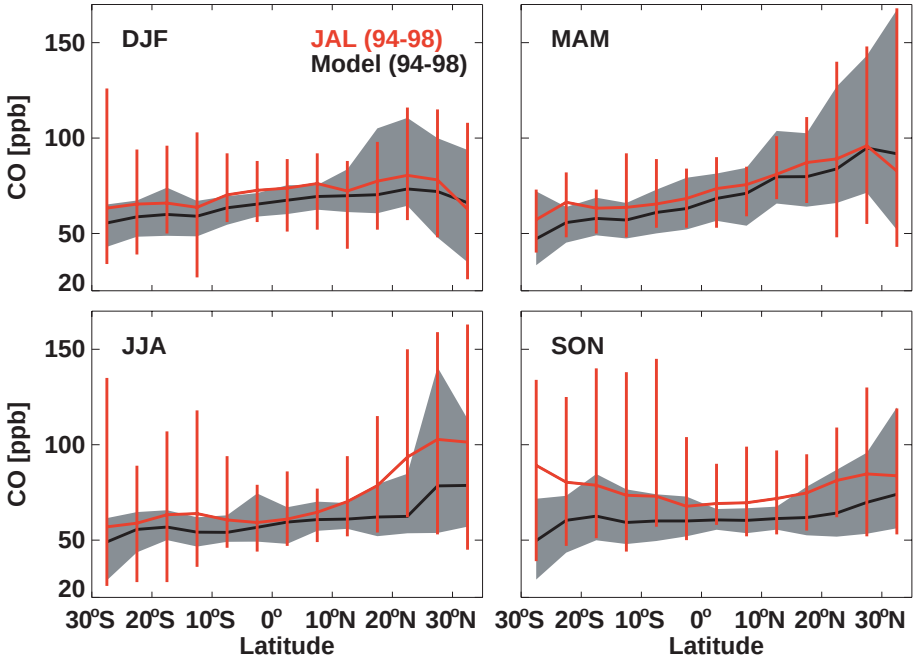


**Fig. 2.** A comparison of the JAL (red) and model (black) CO in the UT (9–13 km) for flights between Tokyo, Japan and Sydney, Australia from 1994-1998, except September 1997 to May 1998. The red vertical bars and gray shaded areas show the range of the observations and model, respectively.

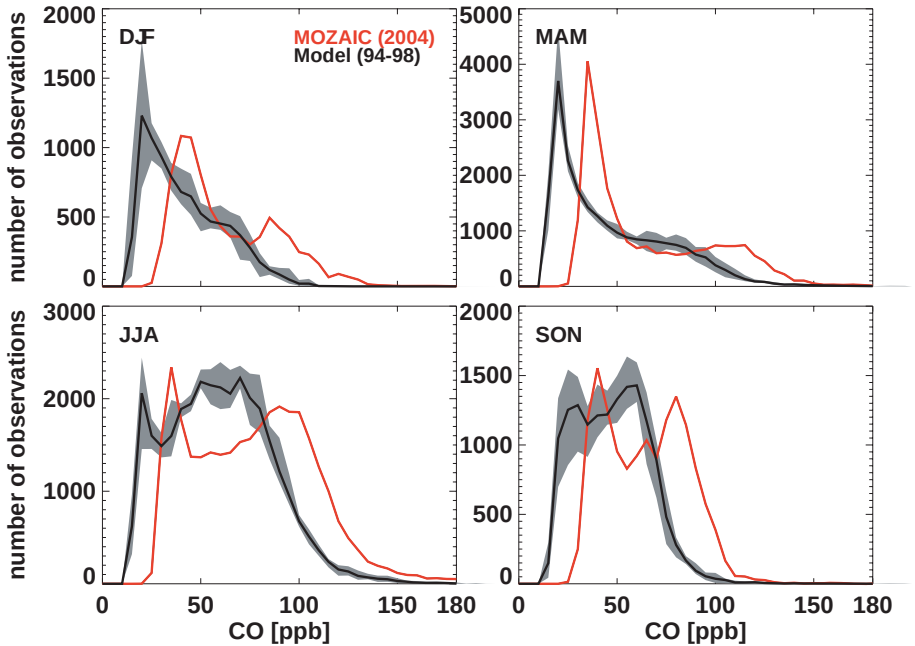


**Fig. 3.** A comparison of the MOZAIC (red) and model (black) CO for flights between East Asia and Europe. The gray shaded area shows the range of the model during 1994–1998. The aircraft data are from 2004.



ACPD
7, 2197–2248, 2007

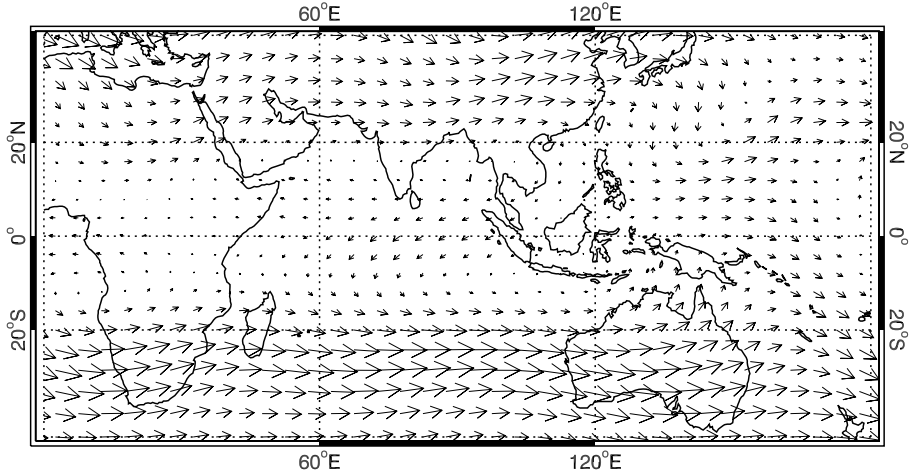


**Fig. 4.** Model winds (m/s) at 200 mb for October 1997.



ACPD
7, 2197–2248, 2007



EGU

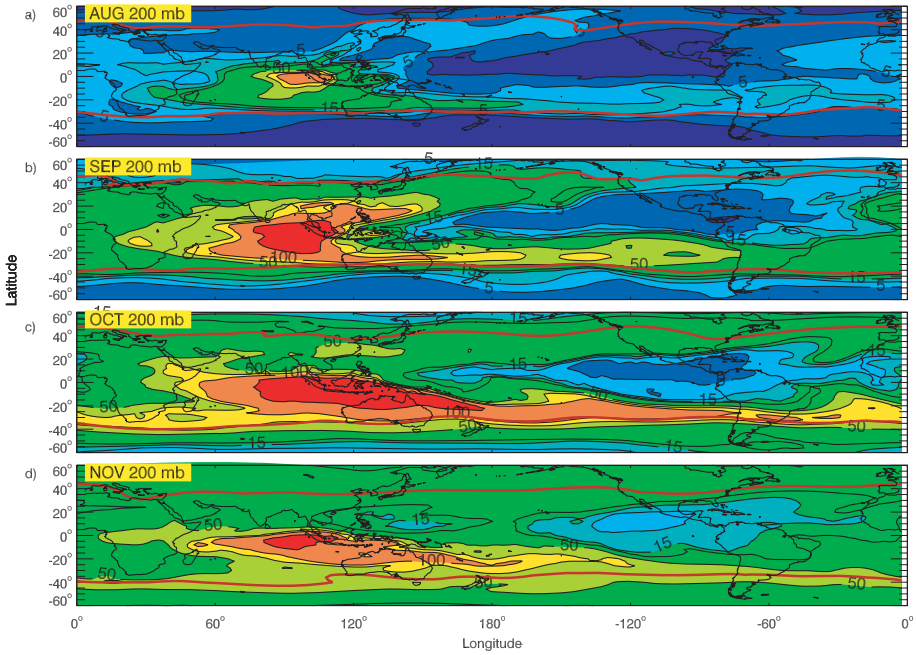


**Fig. 5.** The monthly-averaged CO perturbation (%) for **(a)** August, **(b)** September, **(c)** October, and **(d)** November 1997 caused by the Indonesian fires at 200 mb. The tropopause (red line) is defined by Ertel's potential vorticity ($<3.5\times10^{-6}$ K m$^2$ kg$^{-1}$ s$^{-1}$) or potential temperature (<380 K), whichever gives the higher pressure. The contours are 1, 5, 10, 15, 20, 50, 75, 100, and 200%.



ACPD
7, 2197–2248, 2007



EGU

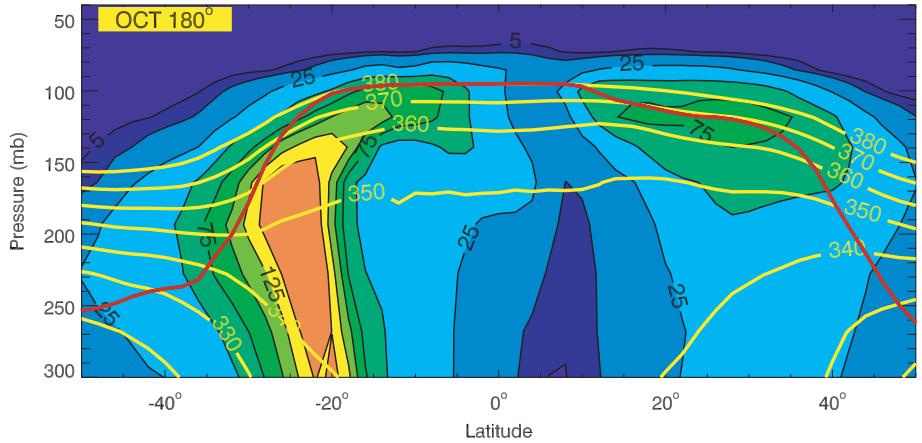


**Fig. 6.** The monthly-averaged CO perturbation (%) at 180° longitude in October 1997 caused by the Indonesian fires. Potential temperatures (K) are shown as yellow lines. The tropopause is shown as a red line. The contours are 5, 10, 25, 50, 75, 100, 125, and 150%.



ACPD
7, 2197–2248, 2007

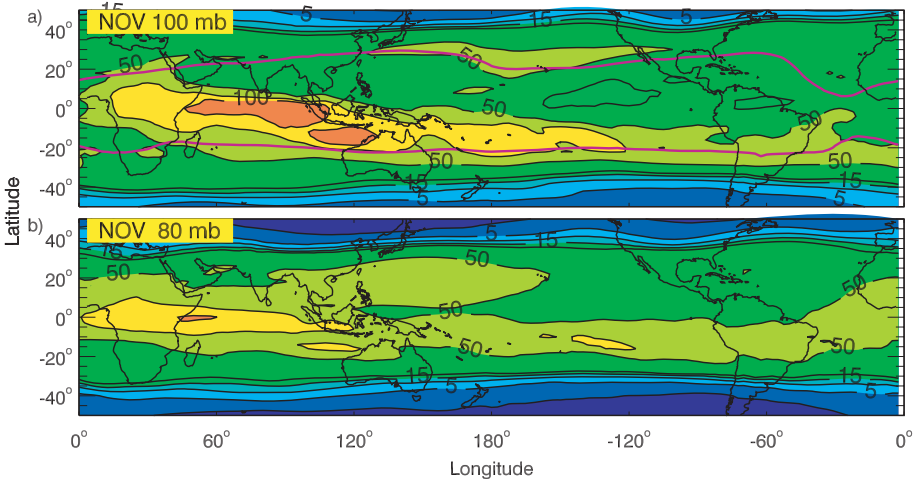


**Fig. 7.** The CO perturbation (%) in November 1997 caused by the Indonesian fires **(a)** near the tropopause and **(b)** in the LS. The 380 K potential temperature (pink line) shows the approximate location of the tropopause. The contours are 1, 5, 10, 15, 20, 50, 75, and 100%.



ACPD
7, 2197–2248, 2007

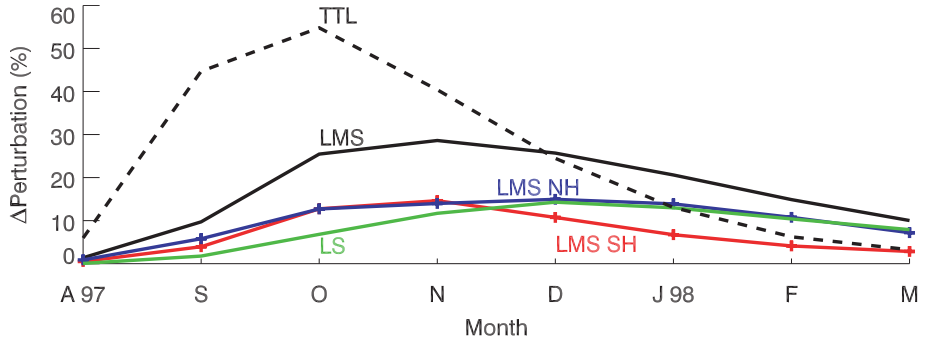


**Fig. 8.** The monthly-averaged mass perturbation of CO (%) in the TTL (dashes), LMS (solid), and LS (green). The portions of the LMS perturbation in the NH (blue crosses) and SH (red crosses) are shown. The TTL is the region below the tropopause (380 K in the tropics), but at pressures <150 mb. The LMS is the region above the tropopause, but below Θ=380 K. The LS is the region above Θ=380 K.



ACPD
7, 2197–2248, 2007

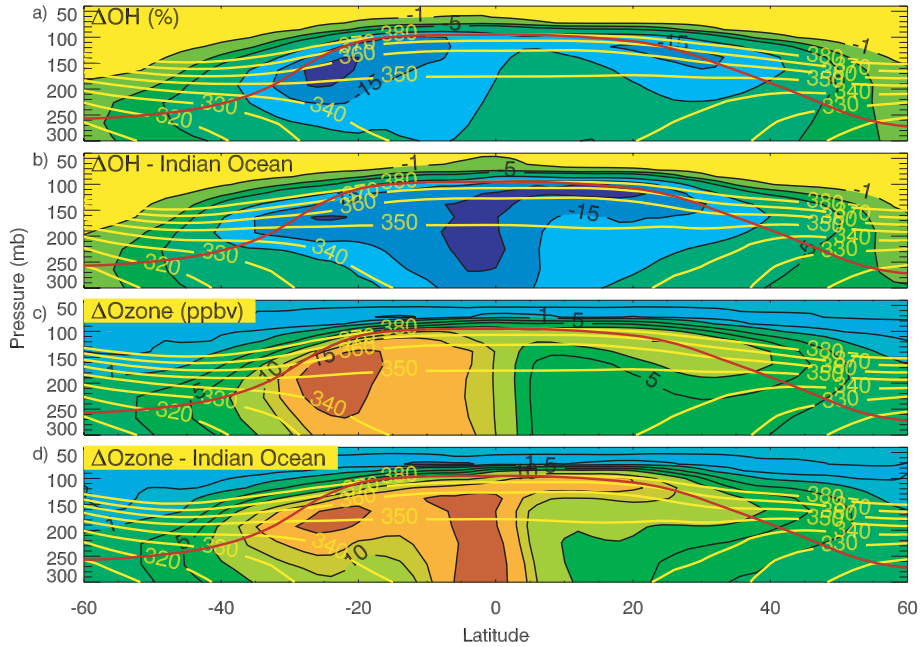


**Fig. 9.** **(a)** The monthly-averaged OH perturbation (%) as a zonal mean for October 1997. **(b)** Same as (b), except for the Indian Ocean region only. **(c)** Same as (a), except for the ozone perturbation (ppbv). **(d)** Same as (c), except for the Indian Ocean region only. Potential temperatures (K) are shown as yellow lines. The tropopause is represented by a red line. The contours for (a) and (b) are –1, –3, –5, –10, –15, and –20% and for (c) and (d) are 1, 3, 5, 7, 10, 12, and 15 ppbv.



ACPD
7, 2197–2248, 2007





EGU

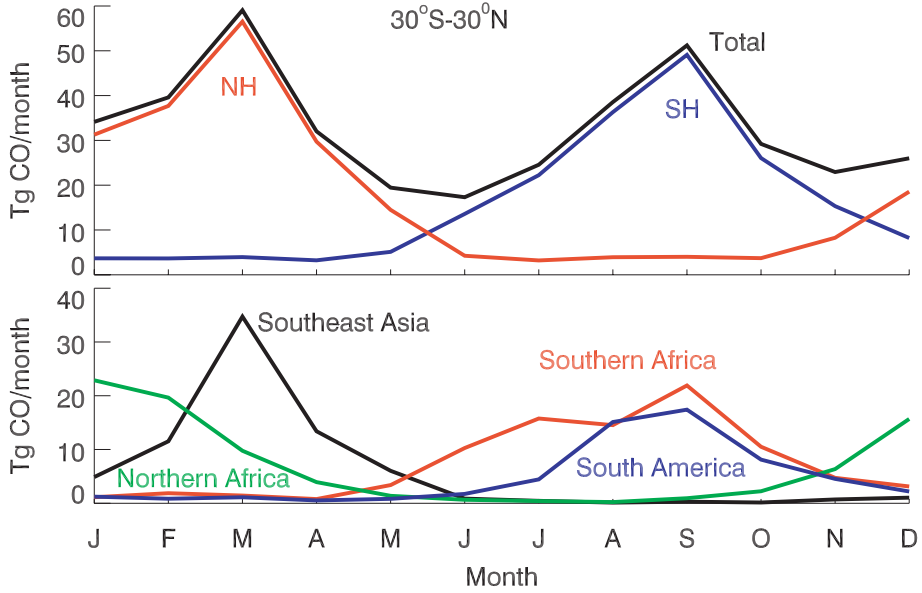


**Fig. 10.** Direct biomass burning emissions (Tg CO/month) from 30°S–30° N (top panel) and by region (bottom panel).



ACPD
7, 2197–2248, 2007

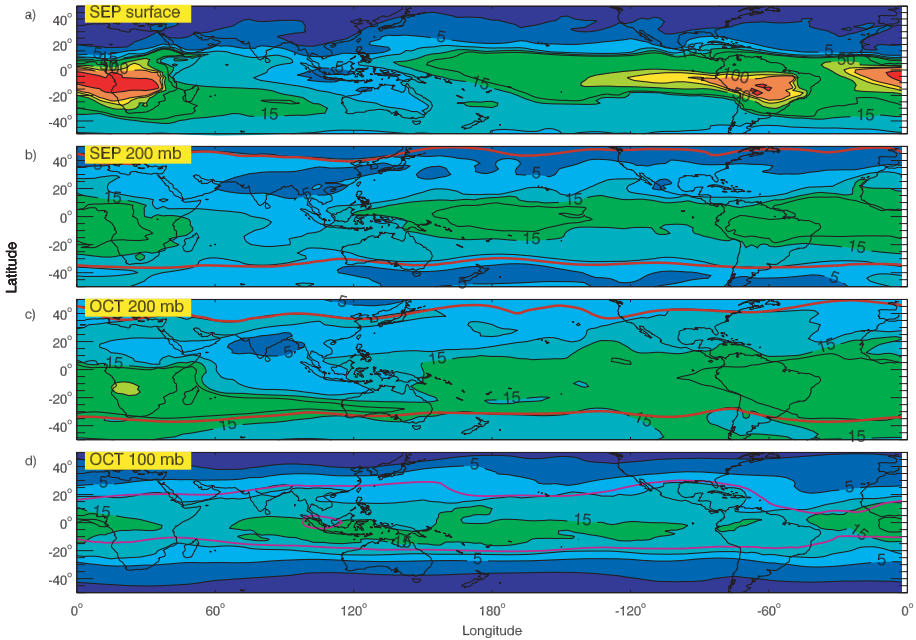


**Fig. 11.** The monthly-averaged CO perturbation (%) for **(a)** September 1994 near the surface, **(b)** September at 200 mb, **(c)** October at 200 mb, and **(d)** October at 100 mb caused by the biomass burning in southern Africa and South America. The tropopause is represented by a red line or the 380 K potential temperature (pink line). The contours are 1, 5, 10, 15, 20, 50, 75, 100, and 200%.



ACPD
7, 2197–2248, 2007

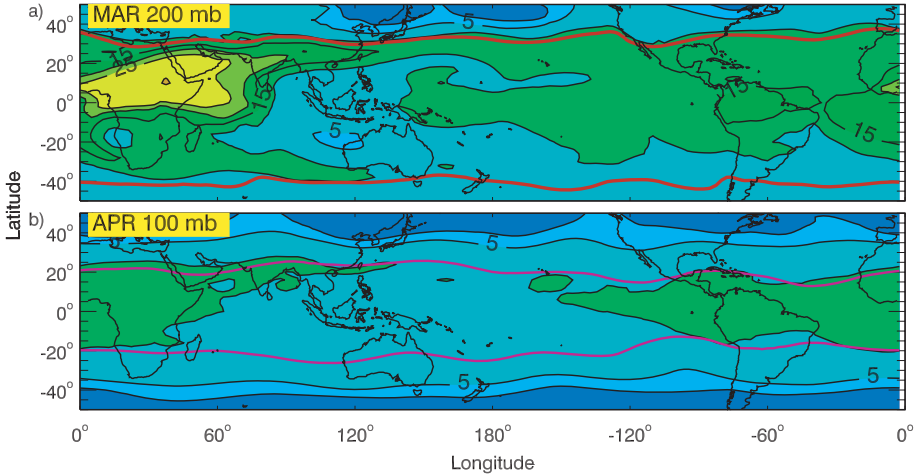


**Fig. 12.** The CO perturbation (%) from biomass burning in northern Africa at **(a)** 200 mb in March and **(b)** 100 mb, near the tropopause, in April, from a model simulation forced by 1995 SSTs. The tropopause is represented by a red line or the 380 K potential temperature (pink line). The contours are 1, 3, 5, 10, 15, 25, and 50%.



ACPD
7, 2197–2248, 2007

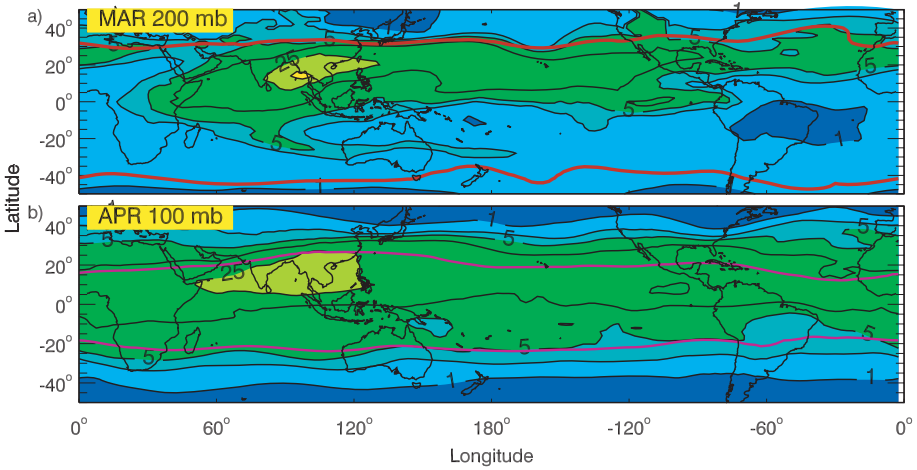


**Fig. 13.** Same as Fig. 12, except for Southeast Asia in 1994.



ACPD
7, 2197–2248, 2007

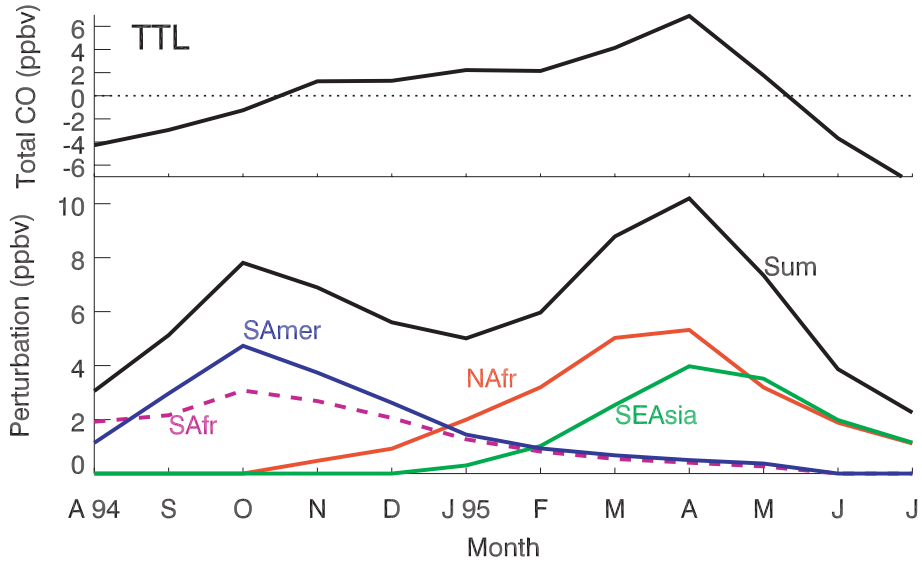


**Fig. 14.** The average CO concentration (ppbv) with the annual mean removed in the TTL (top panel). The CO perturbation (ppbv) from biomass burning in South America (SAmer), southern Africa (SAfr), northern Africa (NAfr), and Southeast Asia (SEAsia). The sum of all four regions is also shown.



ACPD
7, 2197–2248, 2007

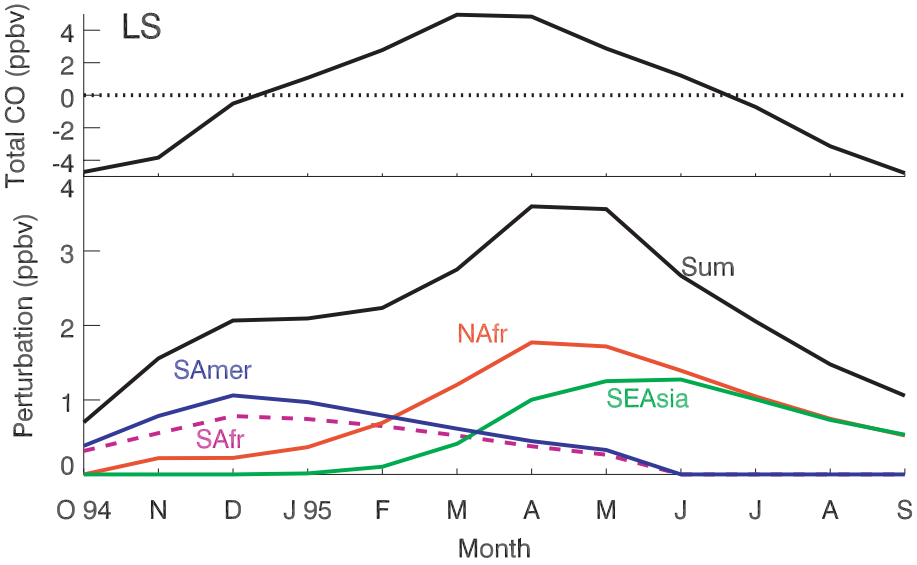


**Fig. 15.** The same as Fig. 14, except for the LS. Note that the x-axis is shifted forward by two months as compared to Fig. 14.



ACPD
7, 2197–2248, 2007

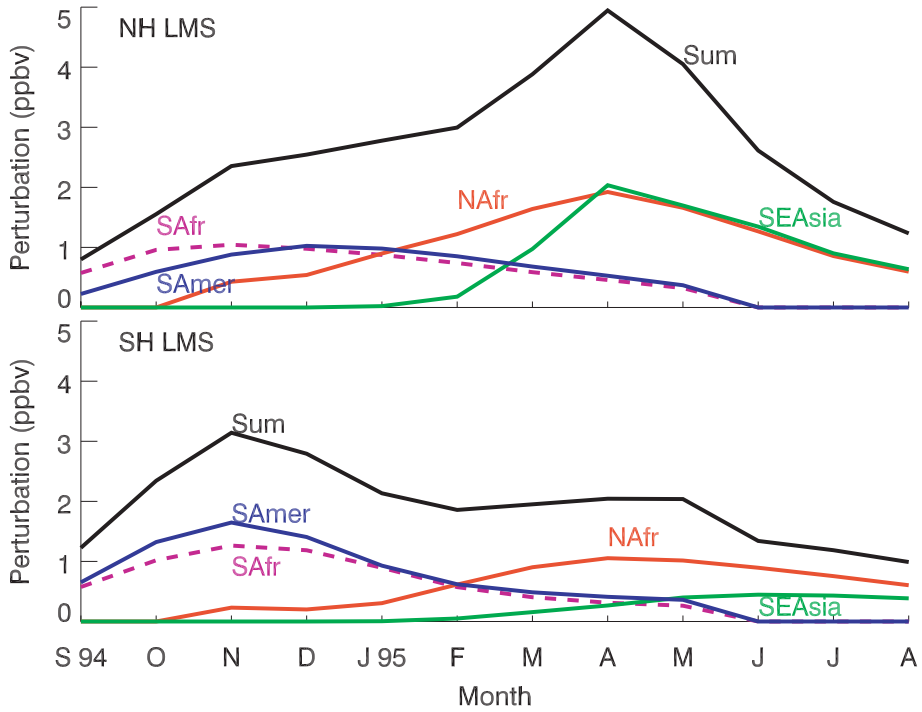


**Fig. 16.** The same as Fig. 14, except for each hemisphere of the LMS. Note that the x-axis is shifted forward by a month as compared to Fig. 14.



ACPD
7, 2197–2248, 2007

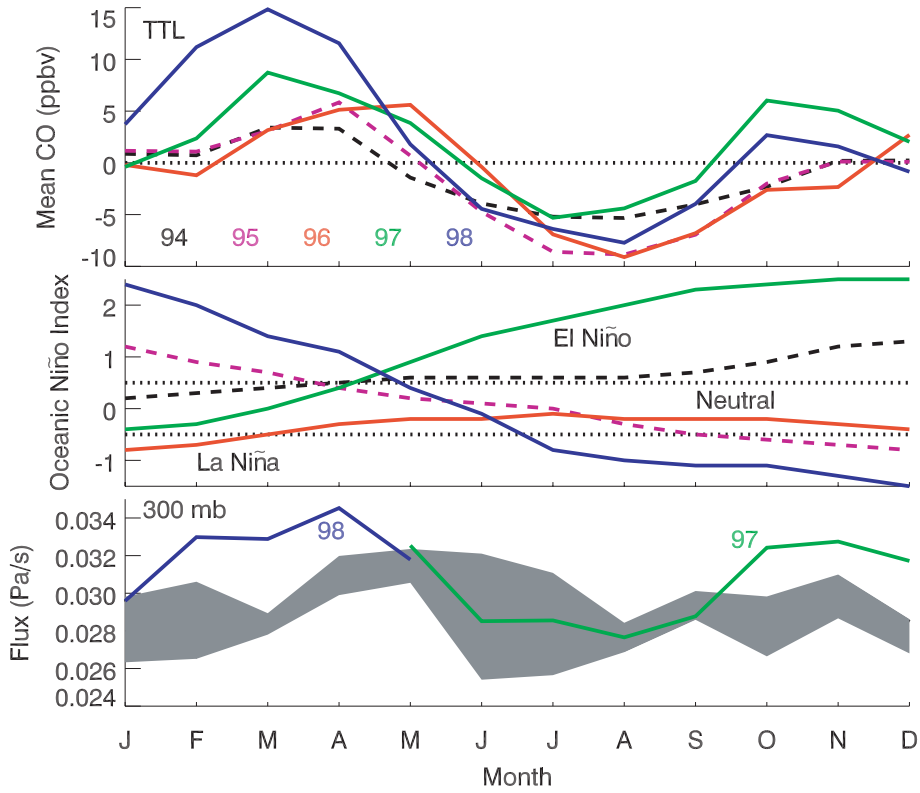


**Fig. 17.** Top: The average CO concentration (ppbv) in the TTL for five years (1994-1998) with the 5-yr mean removed. For clarity, 1994 and 1995 are shown as dashed lines. Middle: The Oceanic Niño Index (degrees) from the Climate Prediction Center of the National Weather Service, taken as 3-month running mean SST anomalies. The threshold is +/–0.5°C for a warm/cold episode. Bottom: The model's mean convective mass flux (Pa/s) at 300 mb from 12° S to 12° N. The shaded area represents the minimum and maximum fluxes during 1994-1998, excluding the 1997/98 El Niño event.